**Title**: Enteroendocrine cell types that drive food reward and aversion

**Authors**: Ling Bai[1,2], Nilla Sivakumar[4], Sheyda Mesgarzadeh[1,2], Tom Ding[1,2], Truong Ly[1,2,3], Timothy V. Corpuz[4], James C.R. Grove[1,2,3], Brooke C. Jarvie[1,2], Zachary A. Knight[1,2,3,4],*

**Affiliations**:
[1]Department of Physiology;
[2]Kavli Institute for Fundamental Neuroscience;
[3]Neuroscience Graduate Program;
[4]Howard Hughes Medical Institute;
University of California, San Francisco; San Francisco, CA 94158, USA
*Corresponding author: zachary.knight@ucsf.edu (ZAK)

**Abstract**:
Animals must learn through experience which foods are nutritious and should be consumed, and which are toxic and should be avoided. Enteroendocrine cells (EECs) are the principal chemosensors in the GI tract, but investigation of their role in behavior has been limited by the difficulty of selectively targeting these cells in vivo. Here we describe an intersectional genetic approach for manipulating EEC subtypes in behaving mice. We show that multiple EEC subtypes inhibit food intake but have different effects on learning. Conditioned flavor preference is driven by release of cholecystokinin whereas conditioned taste aversion is mediated by serotonin and substance P. These positive and negative valence signals are transmitted by vagal and spinal afferents, respectively. These findings establish a cellular basis for how chemosensing in the gut drives learning about food.

## Introduction:

Although the desire to eat is innate, our food choices are driven by learning. Thus, the foods you enjoy today are different from your preferences as a child, in part because you have learned to associate specific flavors with their post-ingestive effects (Sclafani & Ackroff, 2012; Yamamoto & Ueji, 2011). This learning process causes nutrient-rich foods to become more rewarding and toxic substances to become aversive and is critical for guiding animals to choose safe and nutritious food sources in the wild (Myers & Sclafani, 2006). It also contributes to the motivational pull of energy-dense foods in modern society (Johnson, McPhee, & Birch, 1991; Kern, McPhee, Fisher, Johnson, & Birch, 1993). For these reasons, it is critical to establish where in the body ingested nutrients and toxins are detected to drive learning, and whether these parallel processes of food reward and aversion involve dedicated cell types, signals, and pathways.

One of the first sites of post-ingestive chemosensing is the epithelium of the small intestine, which contains a family of specialized sensory cells known as enteroendocrine cells (EECs) (Adriaenssens, Reimann, & Gribble, 2018). EECs exist as multiple subtypes and express receptors and transporters that allow them to monitor the chemical contents of the intestinal lumen. In response to detection of chemical cues, EECs release an array of hormones that include CCK, GIP, GLP-1, PYY, SST, and 5-HT. These molecules can act on local sensory neurons in the lamina propria (Bellono et al., 2017; Kaelberer et al., 2018; Latorre, Sternini, De Giorgio, & Greenwood-Van Meerveld, 2016; Ye et al., 2021) or on distant organs via the circulation to modulate digestion, metabolism and appetite (Adriaenssens et al., 2018; Gribble & Reimann, 2016; Najjar, Davis, & Albers, 2020). Thus, EECs link the detection of chemicals in the gut to the feedback regulation of behavior and physiology.

Given their sensory capabilities, EECs are attractive candidates to drive learning about the post-ingestive effects of different foods. However, investigation of their role in behavior has been hindered by the lack of methods for selectively manipulating these cells in vivo. EECs are sparsely scattered throughout the intestinal epithelium (~1% of cells), undergo rapid turnover (~1 week), and cannot be targeted with viral injections (Polyak et al., 2008). While there are marker genes that distinguish EEC subtypes from each other, these genes are also broadly expressed in other tissues that regulate metabolism and appetite, including, critically, sensory neurons throughout the gut. Thus we lack the capability to directly probe the key nutrient sensors in the GI tract, creating a fundamental gap in our ability to study gut-brain signaling.

70 Here, we describe a general strategy for genetic access to a spectrum of EEC subtypes in vivo. We show that this approach can be used to target actuators to EECs selectively relative to all other cells in the body and thereby control the release of their natural cocktail of hormones at their endogenous sites in the intestine. Using this technique, we show that multiple EEC subtypes inhibit food intake but generate opposing valence signals that create either learned aversion or preference for specific foods. These positive and negative valence signals are transmitted by parallel gut-brain pathways that involve distinct neurotransmitters and afferent sensory neurons. These findings establish a cellular basis for how chemosensing in the GI tract is used to drive learning about food and provide a methodological resource for the further investigation of EEC function in vivo.

80

**Results:**

We first profiled the molecular diversity of EECs in the proximal intestine using single cell RNA sequencing (scRNA-Seq). Due to their sparsity, EECs are difficult to characterize comprehensively even when sequencing is performed on a large scale (Grun et al., 2015; Haber et al., 2017). We therefore enriched for EECs prior to sequencing by labeling all cells derived from the common EEC progenitor using *Neurog3-Cre R26*$^{LSL\text{-}tdTomato}$ mice and then sorting tdTomato+ cells from the small intestine (Figure 1A and Figure 1-figure supplement 1A,B). This lineage-tracing method captures EECs at any stage after differentiation and yielded 7001 cells (with 2168 EECs) for analysis. We then integrated our scRNA-seq data with
90 a complementary dataset (2337 cells with 1244 EECs) that used a pulse-trace reporter *Neurog3*$^{Chrono}$ to transiently label EECs at an early stage after differentiation (Gehart et al., 2019). These two datasets differentially enriched for cell types depending on the timing after differentiation (Figure 1A, 1D and 1E) and together provide more complete coverage of EEC subtypes than either individually.

Unsupervised clustering analysis revealed eight clusters of EECs (Figure 1B, 1C, and 1F), each of which exhibits a unique pattern of chemosensory receptor expression (Figure 1- figure supplement 1). We observed two well-segregated clusters of enterochromaffin cells that correspond to early and late stage cells (EC1 and EC2). These subtypes can be distinguished
100 by the expression of *Tph1/Tac1* or *Tph1/Sct* but do not express any other peptide hormone (Gehart et al., 2019). We also observed three EEC clusters that share high expression of the peptide hormone *Cck* and *Sct*. Two of these clusters correspond to the canonical N/L cells

(*Cck/Gcg/Pyy*) and I cells (CCK), whereas the third uniquely co-expresses *Cck* and *Tph1* (cluster EC/EEC). This third population has not been reported in other recent single-cell sequencing studies but likely corresponds to CCK+/5HT+ cells that have been described immunohistochemically (Reynaud et al., 2016). Finally, we observed well-segregated clusters of D cells (*Sst*), K cells (*Gip*), and X cells (*Ghrl*) that are consistent with previous reports (Gehart et al., 2019). Thus, many canonical EEC subtypes can be differentiated from each other by expression of individual hormones (e.g. EC, D, K, and X cells), whereas others (N/L, I, EC/EEC cells) show partially overlapping hormonal expression.

**An intersectional genetic approach to selectively target EEC subtypes**

While EEC subtypes can be distinguished from other epithelial cells via marker genes (Figure 1C and 1F), the Cre lines corresponding to those genes also label other cell types throughout the body (Figure 2-figure supplement 1). For example, $CCK^{Cre}$ and $Tac1^{Cre}$, which demarcate major subclasses of EECs (discussed below), also label sensory and motor neurons that innervate the intestinal villi (Figure 2D-E). For $CCK^{Cre}$ , this labelling is due to widespread recombination in the enteric nervous system (Figure 2-figure supplement 1C and (Morarach et al., 2021)) whereas $Tac1^{Cre}$ labels subsets of spinal, vagal, and enteric neurons (Browne et al., 2017; Kupari, Haring, Agirre, Castelo-Branco, & Ernfors, 2019; Morarach et al., 2021). This recombination is so widespread that even the focal delivery of light to the intestine would be insufficient to selectively target these EECs for functional manipulations in vivo.

To address this, we developed an intersectional genetic approach for targeting EEC subtypes selectively relative to all other cells in the body (Figure 2A). We first generated a *Villin-Flp* transgenic mouse that efficiently labels the intestinal epithelium (>99%). We extensively characterized the specificity of this line to show that it does not label other tissues, including non-epithelial cells, the nervous system, and visceral organs (Figure 2B-2C), with the exception of rare cells in pancreas (~1%). We then crossed this *Villin-Flp* mouse to Cre drivers that target distinct subsets of cells within the epithelium (described below), such that Flp and Cre act as sequential selectivity filters that together label individual EEC subtypes (Figure 2A, 2F and 2G). Importantly, we confirmed for each Cre driver that it elicits no overlapping recombination in pancreas when combined with *Villin-Flp* (Figure 2-figure supplement 2). Thus, these Cre and Flp drivers can be used in conjunction with dual-recombinase reporter mice to deliver actuators to dispersed EEC subtypes that express both Cre and Flp.

We next assembled a panel of Cre driver mice corresponding to genes expressed in different subsets of EECs, or their progenitors, and characterized their recombination pattern in the intestinal epithelium. Among EEC progenitor markers, we found that *Fev-Cre* efficiently labels all EEC subtypes tested (~90% of cells) but not other cell types in the intestinal epithelium (Figure 2H-2I, and Figure 2-figure supplement 2). Thus, this line enables targeting all EECs simultaneously. In contrast, the progenitor markers *Neurog3-Cre* and *Isl1*$^{Cre}$ labelled other epithelial cells (Figure 1B) or the stem cell niche (Figure 2-figure supplement 2) and therefore lacked useful specificity.

We also tested Cre drivers corresponding to EEC peptide hormones, which revealed that *Tac1*$^{Cre}$, *CCK*$^{Cre}$, and *Sst*$^{Cre}$ label distinct EEC subsets (Figure 2H-2I, and Figure 2-figure supplement 2A). *Tac1*$^{Cre}$ specifically and efficiently labels 5-HT producing enterochromaffin cells, including both early stage (TAC1+, cluster EC.1) and late stage (which have lost TAC1 expression, cluster EC.2) cells but not EECs that express the peptides CCK, GLP-1, GIP, or SST. On the other hand, *CCK*$^{Cre}$ labels virtually all CCK+ cells (~98% in villi) and majority of GLP-1 and GIP expressing cells, consistent with our scRNA-seq data (Figure 1F). Interestingly, we found that subsets of *CCK*$^{Cre}$ labeled EECs also co-express 5-HT (Figure 2H). These cells are distinct from the 5-HT cells derived from the TAC1+ lineage and likely correspond to cluster EC/EEC in our scRNA-seq data (Figure 1B and 1C). A similar recombination pattern to *CCK*$^{Cre}$ was observed for *Gcg*$^{Cre}$. Finally, *Sst*$^{Cre}$ specifically targets D cells (SST+) without any labeling of other cell types. Thus, these Cre drivers can be used in conjunction with *Villin-Flp* to provide efficient and specific genetic access to a spectrum of different EEC subsets.

**Distinct EEC subtypes signal reward and aversion**

We applied this intersectional strategy to manipulate EEC subtypes and investigate how they influence feeding behavior. As hormone release from EECs is naturally triggered by Gq-signaling (Adriaenssens et al., 2018), we targeted the DREADD hM3Dq to EECs (by crossing Cre drivers to *Villin-Flp* and *R26*$^{Dual\text{-}hM3Dq}$ mice) and stimulated these cells with CNO (Figure 3A). We found that CNO activation of all EECs (labelled by *Fev-Cre*) caused a robust reduction of food intake in fasted mice, whereas CNO alone had no effect in littermate controls (Figure 3B and 3C). We further showed that several EEC subtypes were sufficient to inhibit food intake when activated individually, including *Tac1*$^{Cre}$ cells (enterochromaffin cells) as well as *CCK*$^{Cre}$ and *Gcg*$^{Cre}$ cells (I/NL/K cells) (Figure 3B-3C). In contrast, there was no effect on food intake

following stimulation of *Sst*$^{Cre}$ cells (D cells; Figure 3B-3C) or X cells that express ghrelin (via *Ghrl*$^{Cre}$; *R26*$^{LSL\text{-}hM3D}$ mice; Figure 3B-3D). The lack of response in X cells may reflect the fact that ghrelin stimulates feeding only when administered at supraphysiologic levels (~20-fold above baseline, (McFarlane, Brown, Goldstein, & Zhao, 2014)).

We next investigated the ability of EEC subtypes to drive learning about food. We first asked whether pairing EEC activation with consumption of a strongly preferred flavor could create a conditioned taste aversion (CTA). Animals were trained on consecutive days by injection of CNO after sucrose ingestion or vehicle after water ingestion, and then tested for their learned preference (Figure 3E). We found that activation of all intestinal EECs labeled by *Fev-Cre* induced dramatic aversion, such that animals avoided consumption of sucrose after just one training session (Figure 3F) and completely reversed their preference in a subsequent two-bottle test (Figure 3G). This learning was absent in littermate controls (lacking hM3D expression) treated with CNO (Figure 3F-3G). Testing of individual subtypes revealed that activation of *Tac1*$^{Cre}$ labeled enterochromaffin cells alone was sufficient to drive this CTA, whereas activation of other subtypes (labelled by *CCK*$^{Cre}$, *Gcg*$^{Cre}$, or *Sst*$^{Cre}$) created no measurable aversion (Figure 3F-3G).

To test whether activation of these other EEC subtypes may encode positive valence, we next used an assay for conditioned flavor preference (CFP). Mice were trained by allowing them to consume two neutral, non-nutritive flavors, one of which contained CNO and the other vehicle, and learning was accessed by comparing their flavor preference before and after training (Figure 3H). This revealed that activation of EECs labeled by *CCK*$^{Cre}$ or *Gcg*$^{Cre}$ was sufficient to induce robust conditioned preference (Figure 3I), whereas activation of D cells labeled by *Sst*$^{Cre}$ had no effect (Figure 3I). *Fev-Cre* or *Tac1*$^{Cre}$ were not re-tested in this CFP assay, because we had already shown they promote dramatic aversion in the more stringent CTA test (Figure 3F,G). Together, these results reveal that multiple EEC subtypes inhibit food intake but generate opposing valence signals that create learned aversion or preference for specific foods (Figure 3J).

**Different neurotransmitters regulate food consumption and learning**

We next investigated the gut hormones that mediate these effects, by combining chemogenetic activation of EEC subtypes with administration of receptor antagonists. *Tac1*$^{Cre}$ labels enterochromaffin cells that release 5-HT, substance P (encoded by the *Tac1* gene), and

PYY, while *CCK*$^{Cre}$ labels EECs that release CCK, GLP-1, GIP, PYY, and 5-HT (Figure 2H-2I, and Figure 2-figure supplement 1A). We therefore tested a panel of antagonists targeting key receptors for these hormones, including ondansetron (for 5-HT3R), RP67580 (for TACR1) and JNJ-31020028 (for the PYY receptor NPY2R), Devazepide (for CCKAR) and Ex3 (for GLP1R).

We found that the acute inhibition of feeding caused by enterochromaffin cell stimulation (*Tac1*$^{Cre}$) was attenuated by treatment with an antagonist targeting 5-HT3R but not TACR1 or NPY2R (Figure 4A and Figure 4-figure supplement 1A). Interestingly, although 40% of *CCK*$^{Cre}$ EECs also secrete 5-HT (Figure 2I), a 5-HT3R antagonist had no effect on the inhibition of feeding caused by *CCK*$^{Cre}$ EECs. In contrast, this feeding inhibition was fully blocked by antagonists against either CCKAR or NPY2R, but not TACR1 or GLP1R (Figure 4B and Figure 4-figure supplement 1B). Thus, although the hormones released by *Tac1*$^{Cre}$ EECs and *CCK*$^{Cre}$ EECs are partially overlapping, the receptors required for their acute inhibition of feeding are different (5-HT3R for *Tac1*$^{Cre}$ EECs, versus CCKAR and NPY2R for *CCK*$^{Cre}$ EECs) (Figure 4E). This suggests that the same gut hormone can have different effects when released by different cell types.

To investigate how these signals drive learning, we treated animals with the same panel of antagonists during taste conditioning. We found that inhibition of 5-HT3R or TACR1 during training could partially block the CTA induced by enterochromaffin cell activation, whereas the NPY2R antagonist had no effect (Figure 4C and Figure 4-figure supplement 1E). Strikingly, combined treatment with 5-HT3R and TACR1 antagonists during training abolished the enterochromaffin cell induced CTA (Figure 4C and Figure 4-figure supplement 1E). Similar effects were observed for the CTA induced by activation of all EECs (Figure 4-figure supplement 1C,D). Thus, enterochromaffin cells can induce learned aversion by signaling through the 5-HT3R and TAC1R, whereas their acute inhibition of feeding requires only 5-HT/5-HT3R signals (Figure 4E).

We performed a similar analysis for the effects of *CCK*$^{Cre}$ cells. Since CCKAR and NPY2R are required for the feeding inhibition induced by *CCK*$^{Cre}$ cells, we tested whether these receptors are necessary for flavor conditioning by administering antagonists during training. We found that flavor preference induced by *CCK*$^{Cre}$ cell stimulation was prevented by blocking CCKAR but not NPY2R (Figure 4D). The fact that NPY2R antagonists can block *CCK*$^{Cre}$ induced

satiety, but not flavor preference, reveals these cells influence satiety and learning through separable mechanisms (Figure 4E).

240

**Parallel neuronal pathways convey EEC signals to the brain**

We sought to identify how this information is transmitted to the brain. Vagal and spinal afferents comprise the two major ascending circuits for gut-brain communication (Brookes, Spencer, Costa, & Zagorodnyuk, 2013; Latorre et al., 2016), and subsets of these sensory neurons express receptors for hormones released by EECs, including 5-HT3R, CCKAR, and NPY2R (Bai et al., 2019; Li et al., 2016; Sharma et al., 2020; Williams et al., 2016). We therefore tested the necessity of these two pathways for the effects of EECs on learning and appetite.

250 We prepared cohorts of triple transgenic mice for chemogenetic activation of *CCK*$^{Cre}$ or *Tac1*$^{Cre}$ labeled cells, and then subjected these animals to one of two procedures (Figure 5A): subdiaphragmatic vagotomy to surgically remove vagal innervation to the abdominal viscera (Figure 5-figure supplement 1A and B) or intrathecal injection of resiniferatoxin (RTX), a potent TRPV1 agonist, to ablate TRPV1+ spinal afferent neurons without impacting vagal sensory neurons (Figure 5-figure supplement 1C and D) (Mishra & Hoon, 2010). We then measured the effect of chemogenetic stimulation of EECs in these deafferented animals and controls.

We found that vagotomy abolished the feeding inhibition induced by activation of *CCK*$^{Cre}$ labeled EECs (Figure 5C and S5F) but had no effect on the reduction in feeding induced by
260 *Tac1*$^{Cre}$ EECs (Figure 5B and S5E). In contrast, intrathecal RTX treatment abolished the feeding inhibition induced by the *Tac1*$^{Cre}$ labeled EECs (Figure 5D and S5G) but had no effect on responses to *CCK*$^{Cre}$ EECs (Figure 5E and S5H). Thus, the EECs labeled by *Tac1*$^{Cre}$ and *CCK*$^{Cre}$ inhibit food intake via spinal and vagal pathways, respectively (Figure 5H).

We next investigated how these two neuronal pathways contribute to EEC driven learning. Intrathecal RTX prior to training was sufficient to partially prevent the acquisition of CTA following *Tac1*$^{Cre}$ activation, indicating that spinal afferents contribute to this process (Figure 5F), whereas vagotomy prior to training did not block this CTA (as reflected by the reduction in sucrose intake after one round of training; Figure 5F and S5I). In contrast, the conditioned
270 flavor preference induced by the *CCK*$^{Cre}$ activation was unaffected by the ablation of TRPV1+ spinal afferents but abolished by vagotomy (Figure 5G). Thus, vagal afferents are necessary

for the *CCK*$^{Cre}$ EECs to transmit positive valence to the brain, whereas enterochromaffin cell mediated aversion is relayed at least in part by spinal pathways (Figure 5H).

**Discussion:**

EECs are the proximal sensors of most chemical cues in the GI tract and consequently play a privileged role in gut-brain communication. However, direct tests of their function have been limited by the difficulty of selectively accessing these cells for manipulations in vivo. One recent study used the gene Insl5 to target GLP1/PYY+ EECs in the colon (Lewis et al., 2020), but most marker genes that label EEC subtypes are broadly expressed in other tissues important for metabolism and appetite (Figure 2-figure supplement 1). As a result, EECs have not been subject to the kinds of acute and targeted manipulations that have been critical for unravelling how circuits in the brain and peripheral nervous system control feeding behavior.

Here, we have described a general strategy for genetic access to a spectrum of EEC subtypes for functional manipulations in behaving mice. This approach uses Flp and Cre drivers as sequential selectivity filters to progressively restrict transgene expression to the intestinal epithelium and then to cell types within that structure. This makes it possible to target rare EEC subsets (each <1% of epithelial cells) with high efficiency (>90% labelling) and undetectable recombination in off-target tissues. Importantly, these tools can be combined with a variety of existing dual recombinase reporter mice to deliver actuators (e.g. DREADDs or opsins) to different EEC subsets, thereby opening the door to systematic functional exploration of these cells in vivo.

For this study, we assembled a panel of Cre drivers that label either all EECs (*Fev-Cre*) or non-overlapping subsets that collectively span much of EEC diversity (*CCK*$^{Cre}$, *Tac1*$^{Cre}$, *Sst*$^{Cre}$ and *Ghrl*$^{Cre}$). While these markers define canonical EEC subtypes, other classes of Cre drivers could be used to investigate cross-sections of EECs that vary along different dimensions. For example, the expression of nutrient receptors and transporters may define EEC subpopulations that have a shared chemosensory function (Figure 1C and Figure 1-figure supplement 1F). Similarly, in this study we have not explored how the function of these molecularly-defined EEC subsets varies with location in the intestine, but this could be addressed by combining the genetic approach described here with tools for wireless optogenetics in visceral organs (Park et al., 2015).

**Manipulations of hormones versus cell types**

Our understanding of how EECs modulate behavior is based primarily on studies of the hormones they produce (Adriaenssens et al., 2018; Clemmensen et al., 2017; Myers & Sclafani, 2006). While much has been learned from this pioneering work, all EECs express more than one hormone (Fothergill & Furness, 2018; Grunddal et al., 2016; Habib et al., 2012; Sykaras et al., 2014), and these hormone cocktails are not released directly into blood but rather into the intestinal mucosa in the vicinity of the axons of vagal and spinal afferents (Latorre et al., 2016; Najjar et al., 2020). Some EECs likely form direct synaptic connections with these afferent terminals (Bellono et al., 2017; Kaelberer et al., 2018), and different hormones can be packaged into distinct vesicle pools within the same EEC (Fothergill, Callaghan, Hunne, Bravo, & Furness, 2017; Fothergill & Furness, 2018). This spatial and functional organization of EECs within the lamina propria creates potential mechanisms for the same hormone to have different effects depending on where it is released.

We investigated this by directly stimulating EEC subtypes in vivo and measuring the effect on behavior, which revealed many instances of divergence between EEC activation and hormone pharmacology. For example, we found that direct stimulation of *CCK*$^{Cre}$ cells both inhibits feeding and produces robust conditioned flavor preference (Figure 3I), despite the fact that systemic injection of many of the individual hormones produced by these cells induces aversion at doses that inhibit food intake (Chelikani, Haver, & Reidelberger, 2006; Deutsch & Hardy, 1977; Ervin, Birkemo, et al., 1995; Ervin, Carter, Webster, Moore, & Cooper, 1984; Halatchev & Cone, 2005; Kanoski, Rupprecht, Fortin, De Jonghe, & Hayes, 2012). We also found that the same hormone produced by different EECs can have different functions. For example, a PYY receptor antagonist blocked the anorexia produced by stimulation of *CCK*$^{Cre}$ cells but not *Tac1*$^{Cre}$ cells, even though PYY was expressed by subsets of both EECs (Figure 4A and 4B). Conversely, a 5-HT3R antagonist blocked the anorectic effect of stimulating *Tac1*$^{Cre}$ but not *CCK*$^{Cre}$ EECs (Figure 4A and 4B), although many *CCK*$^{Cre}$ EECs also produce 5-HT (Figure 2I). These observations are consistent with the idea that EEC signaling is highly organized within the lamina propria, such that neurotransmitters released by EEC subtypes are funneled to specific sensory pathways. The ability to selectively access EEC subtypes for genetic manipulations will enable further studies that map these visceral circuits.

**Gut-brain pathways for food reward and aversion**

Post-ingestive signals shape our decisions about what to eat and can override innate preferences, such that animals learn to prefer bitter foods that are nutritious and avoid sweet substances that are toxic (Kern et al., 1993; Lin, Arthurs, & Reilly, 2017; Myers & Sclafani, 2006). The gut epithelium is the interface between ingested food and the body and is poised to provide feedback about ingested food that drives learning. However, it has been unclear to what extent there are dedicated sensors in the epithelium that encode the values of ingested substances and drive food preference versus aversion. We therefore investigated the role of EEC subtypes in this process of learning about food.

The major finding from these experiments was that stimulation of two different EEC types was sufficient to drive either food preference or aversion, and that the effects of these cells were mediated by parallel gut-brain pathways that involve distinct hormones and afferent nerves. Acquisition of food preference was driven by stimulation of EECs labelled by *CCK*$^{Cre}$ or *Gcg*$^{Cre}$ and was blocked by antagonists against CCKAR but not any other hormone produced by these cells. Of note, prior work has shown that CCK injections can induce flavor preference at low doses that do not affect feeding (Perez & Sclafani, 1991) and aversion at higher doses (Deutsch & Hardy, 1977; Ervin, Birkemo, et al., 1995; Ervin, Mosher, Birkemo, & Johnson, 1995). Our data show that direct stimulation of *CCK*$^{Cre}$ cells can simultaneously produce both satiety and food reward.

The effect of *CCK*$^{Cre}$ cells on satiety and food preference required intact vagal afferents, but not spinal afferents, which is consistent with an extensive literature showing that the vagus nerve mediates many of CCK's effects (Joyner, Smith, & Gibbs, 1993; Raybould, 2007; Smith, Jerome, Cushin, Eterno, & Simansky, 1981). The CCKAR is expressed in multiple vagal subtypes, including IGLE mechanoreceptors that innervate the stomach (Glp1R+) and intestine (OxtR+) (Bai et al., 2019; Williams et al., 2016). These IGLE subtypes inhibit food intake when stimulated (Bai et al., 2019) and are required for the reduction in feeding following CCK injection (Borgmann et al., 2021) and therefore likely contribute to the effects of *CCK*$^{Cre}$ EECs on food intake. It is less clear which vagal cells mediate CCK's effects on flavor preference, although stimulation of all gut-innervating vagal afferents is reinforcing (Han et al., 2018). One plausible candidate is the Vip+/Uts2b+ vagal neurons that innervate the intestinal mucosa and express high levels of CCKAR but do not inhibit food intake when stimulated (Bai et al., 2019).

Peripheral 5-HT has been implicated in numerous processes including GI motility, secretion, vasoconstriction, bone growth, inflammation, visceral malaise, metabolism, and appetite (Mawe & Hoffman, 2013; Spohn & Mawe, 2017). Enterochromaffin cells are the major source of 5-HT in the gut, and we found that direct stimulation of *Tac1*$^{Cre}$ labelled enterochromaffin cells acutely inhibited food intake and caused dramatic CTA. The inhibition of food intake required 5-HT signaling, whereas the CTA could be fully prevented only by simultaneously blocking receptors for two hormones produced by these cells during training (5-HT3R and TACR1). This is consistent with the hypothesis that some biological functions of EECs are encoded in their ability to release cocktails of hormones with redundant functions.

Intestinal serotonin can activate both vagal and spinal pathways, but we found that only spinal afferents were required for the reduction in food intake and CTA triggered by stimulation of enterochromaffin cells. This may be mediated by 5-HT3R-expressing spinal afferents that innervate the distal intestine (Hockley et al., 2019), are functionally coupled to enterochromaffin cells (Bellono et al., 2017), and are poised to transmit aversive visceral signals (such as abdominal pain) that are sensitive to 5-HT3R antagonists (Ford et al., 2009; Gebhart & Bielefeldt, 2016). Of note, many vagal sensory neurons also express 5-HT3Rs, and our findings do not rule out a role for those cells in nausea (Babic & Browning, 2014) or non-aversive satiety (Savastano & Covasa, 2007). However, we did not observe either aversion or 5-HT3R-sensitive anorexia following stimulation of *CCK*$^{Cre}$ EECs (which act via the vagus and also produce 5-HT). The ability to manipulate EEC subtypes in vivo should enable further studies that investigate how these pathways coordinate diverse physiology using a small set of neurochemical signals.

## Materials and Methods

### Animals

Animals were maintained in temperature- and humidity-controlled facilities with 12 hours light-dark cycle and ad libitum access to water and standard chow (PicoLab 5053). We used the following transgenic mice, all of which were on a C57Bl/6J background: *Cck*$^{Cre}$ (JAX 012706), *Gcg*$^{Cre}$ (JAX 030542), *Tac1*$^{Cre}$ (JAX 021877), *Sst*$^{Cre}$ (JAX 028864), *Ghrl*$^{Cre}$ (JAX 029260), *Fev-Cre* (JAX 012712), *NeuroG3-Cre* (JAX 006333), *ROSA26Sor*$^{tm14(CAG\text{-}tdTomato)Hze}$ (JAX 007914), *ROSA26Sor*$^{tm3.2(CAG\text{-}EGFP,\text{-}CHRM3*/mCherry/Htr2a)Pjen}$ (JAX 026942), *Igs7*$^{tm162.1(tetO\text{-}GCaMP6s,CAG\text{-}tTA2)Hze}$ (JAX

031562), and *Vil-Flp* (this study). Mice were at least six weeks old at the time of surgery. All studies employed a mixture of male and female mice and no differences between sexes were observed. All experimental protocols were approved by the University of California, San Francisco IACUC following the National Institutes of Health guidelines for the Care and Use of Laboratory Animals.

Generation of Villin-Flp transgenic mice

The *Villin-Flp* allele was generated by pronuclear microinjection of *Villin-Flp-WPRE-pA* transgene. Briefly, the 12.4kb-Villin promoter was acquired from Addgene (12.4kb Villin-ΔATG, Plasmid #19358). This promoter has been demonstrated to drive expression specifically in the intestinal epithelium and not in other tissues (*1*). After XmaI/XhoI linearization, a *Flpo-WPRE-hGH polyA-EcoR1* fragment was inserted after the *Villin* promoter using Gibson Cloning to generate *Villin-Flp-WPRE-polyA* flanked by EcoR1.

The construct was linearized by EcoR1 and prepared for pronuclear microinjection at the UCSF Gladstone Transgenic Gene-Targeting Core Laboratory. 120 injected embryos were implanted into pseudopregnant CD1 female mice. 7 out of 31 pups contained the Flp cassette and could transmit it to the next generation. Those 7 founders were crossed to Flp-dependent reporter *RC::FLTG* (Jackson 026932) to characterize the pattern of Flp-mediated recombination. 2 out of 7 founders induced efficient recombination in the intestinal epithelium with very sparse labeling of the pancreatic cells (~1%), and one of them was kept as the *Villin-Flp* line and used for this study. The other 5 founder lines were eliminated, including 3 founders with good intestinal labeling as well as high-recombination in the pancreas (~90%), and 2 founders with poor recombination in the intestine. The *Villin-Flp* line was backcrossed to C57BL/6J for more than 6 generations and was maintained on C57BL/6J background.

Generation of EEC scRNA-seq dataset (lineage-trace strategy)

Four 6-week old *Neurog3-Cre; Rosa*$^{LSL\text{-}tdTomato}$ mice (2 males and 2 virgin females) were used for the scRNA-Seq preparation. Mice were anesthetized under isoflurane and then euthanized via cervical dislocation. Small intestines were harvested and cleaned in HBSS. Crypts and villi were isolated by 1mM EDTA in HBSS (without $Ca^{2+}$, $Mg^{2+}$) for 10min, mechanically detached, and pelleted. The crypt and villus pellets were then resuspended in warm digestion solution (2.5% Trypsin in HBSS) and incubated for 20 mins, pelleted, washed with MEM, and triturated with a P1000 pipette. The suspended cells were filtered through a 40 μm cell strainer, pelleted

440 again and resuspended in FACS buffer (0.1% BSA in PBS). TdTomato$^+$ cells were collected using flow cytometry (yield 0.6-0.8% of total cells), and 198.5k cells were suspended in 100ul FACS buffer to reach a density of 2000 cell/uL for sequencing.

Single cells were processed through the GemCode Single Cell Platform using the GemCode Gel Bead, Chip and Library Kits (10X Genomics, Pleasanton) as per the manufacturer's protocol. Single-cell cDNA libraries were sequenced on the Illumina Highseq 4000. De-multiplexing alignment to the mm10 transcriptome and unique molecular identifier (UMI)-collapsing were performed using Cell Ranger version 2.0.1, available from 10X Genomics with default parameters. A gene-barcode matrix was generated. 0.3 billion reads over 7701 cells
450 were captured, with 39.5 thousand mean reads per cell and 1.8 thousand median genes per cell.

Integrated analysis of EEC scRNA-Seq datasets

To pre-process the EEC scRNA-seq datasets, the feature-barcode matrices were loaded into Seurat (v3) following standard workflow. For the lineage-trace dataset (generated in this paper), cells that fulfilled the following criteria (7001 cells covering 18173 genes) were included for analysis: 1) percentage of mitochondrial reads < 10%; 2) number of genes > 1000. For the pulse-trace dataset (*2*), cells that fulfilled the following criteria (2405 cells covering 20751 genes) were included for analysis: 1) percentage of mitochondrial reads < 10%; 2) number of
460 genes > 250 and < 9000; 3) number of reads > 2000 and < 100000.

The filtered scRNA-seq datasets (lineage-trace and pulse-trace) were further integrated using Seurat's IntegrateData function (anchors = 2000, dimensions = 1:40). Non-EEC epithelial cell types were identified based on published marker genes (*3*, *4*), including progenitors (*Neurog3*$^+$), enterocytes (*Fabp1*$^+$, *Reg1*$^+$), goblet cells (*Guca2a*$^+$, *Muc2*$^+$), Paneth cells (*Lyz1*$^+$, *Defa17*$^+$), and tuft cells (*Dclk1*$^+$, *Trpm5*$^+$) (Figure 1-figure supplement 1F).

Perfusion and tissue preparation

Mice were anesthetized under isoflurane and then transcardially perfused with 10 ml PBS
470 followed by 15 ml formalin (10%). Brain, vertebral column, and visceral organs were dissected, post-fixed in 10% formalin overnight at 4ºC, and washed 3x20 min with PBS at RT. Tissues were kept in PBS at 4ºC before imaging, sectioning, or staining. For imaging myenteric ganglia (Figure 2-figure supplement 1), the duodenum was dissected, pinned flat in 10% formalin and

stored overnight at 4°C. After being rinsed 2x15 min in PBS at RT, the muscle layer was dissected away from the submucosa using a dissecting scope and sharp forceps. The muscle layer containing the myenteric ganglia was stored free-floating in PBS at 4°C until immunohistochemistry. for 2h at RT.

Immunohistochemistry

Tissues were cryoprotected with 30% sucrose in PBS overnight at 4ºC, embedded in OCT, frozen and stored at -20ºC. Sections (30 um for peripheral tissues, or 50 um for the brain) were prepared with a cryostat and collected in PBS or on Superfrost Plus slides. Sections were washed 3×10 min with 0.1% PBST (0.1% Triton X-100 in PBS), blocked (5% NGS or NDS in 0.1% PBST) for 30 min at RT, and incubated with primary antibodies (diluted in blocking solution) overnight at 4ºC. For HuC/D staining of myenteric ganglia, primary antibody was incubated for 72 hours at 4°C. The next day, sections were washed 3x10 min with 0.1% PBST, incubated with secondary antibodies (1:500 diluted in blocking solution) for 2 hours at RT, washed again 3×10 min with 0.1% PBST, and mounted using fluoromount-G with DAPI (Southern Biotech).

Primary antibodies used were: chicken anti-GFP (Abcam, ab13970, 1:1000), rabbit anti-GFP 1:1000 (LifeTech, A11122), goat anti-mCherry (ACRIS, AB0040-200), Rabbit anti-5-HT 1:2000 (Immunostar, 20080), Rabbit anti-CCK 1:500 (Millipore/Sigma,C2581), Rabbit anti-ChgA 1:1000 (Immunostar, 20085), Rabbit anti GIP 1:500 (Abcam, ab22624), Mouse anti Glp1 1:200 (Abcam, ab26278), Rabbit anti PYY 1:500 (Abcam, ab22663), Rat anti-SST 1:200 (Millipore, MAB354), Rat anti-Substance P (TAC1) 1:200 (Abcam, ab7340), Guinea pig anti-TRPV1 1:500 (Millipore, AB5566), and rabbit anti-HuC/D 1:500 (Abcam, ab210554)

Image acquisition

All histology images were taken by confocal microscopy (Zeiss, LSM 510) as previously described (Bai et al., 2019).

Subdiaphragmatic vagotomy

Mice were anaesthetized with ketamine/xylazine delivered intraperitoneally (100 mg/kg Ketamine with 10 mg/kg Xylazine). A 1-2 cm incision was made along the medial line beginning at the distal edge of the sternum. The liver was then retracted with sterile cotton swabs that had been moistened with saline so that the distal end of the esophagus could be

visualized. Both branches of the vagus nerve were isolated from the esophagus and a 1–2-mm section of each branch of the nerve was resected with scissors. Control mice for vagotomy experiments underwent a sham surgery that included internal organ manipulation but not vagotomy. To maintain gastrointestinal flow after vagotomy surgery, mice were kept on a mixed liquid diet (Enfamil, ASIN B004L5L5TA) and solid diet (standard chow, PicoLab 5053). Mice were allowed to rest for 2-3 weeks before used for behavior experiments.

To validate the subdiaphragmatic vagotomy, mice received an intraperitoneal injection of wheat germ agglutinin conjugated to Alexa Fluor 488 (WGA-488, 5mg/kg, dissolved in PBS) and were euthanized four days later. WGA-488 is taken up by axon terminals of intact vagal motor neurons, the somas of which are located in the dorsal motor nucleus of the vagus (DMV) of brainstem and can be visualized by histology (Figure 5-figure supplement 1A and B). Labelling in the dorsal motor nucleus of the vagus was greatly reduced by subdiaphragmatic vagotomy.

IT-RTX injection

For ablation of TRPV1$^+$ DRG neurons, 6- to 8-week-old mice were injected intrathecally with RTX (50 ng/mouse). Briefly, mice were lightly held and a 30G needle attached with Hamilton syringe was inserted at the L6-S1 vertebral junction. For the RTX group, 10 ul of RTX (5 ng/ul in ethanol) was injected to reach a dose of 50 ng/mouse. For the vehicle control group, 10 ul of ethanol was injected instead. Mice were allowed to rest for 3 weeks before being used for behavior experiments. Successful treatment was confirmed by a loss of TRPV1$^+$ neurons in the DRG, as well as reduction of TRPV1$^+$ signals of the superficial lamina of spinal cord dorsal horn (Figure 5-figure supplement 1C and D).

Post-surgical care

Post-surgery mice were placed over a heating pad and monitored for their recovery from anesthesia. The health of the mice was monitored daily post-surgery. All mice were given post-surgery analgesia by subcutaneous injection of meloxicam (5 mg/kg) on post-surgery day 2 and day 3.

Behavioral equipment

All experiments were performed in behavioral chambers (Coulbourn Instruments, Habitest Modular System). Feeding experiments were performed using a pellet dispensing system

(Coulbourn, H14-01M-SP04 and H14-23M) with free water access. Food pellets (20 mg Bio-Serv F0163) were dispensed at the beginning of trials, or after pellet removal with a 10 sec interval. Consumption of water or other liquid solution was monitored with contact lickometers (Slotnick, 2009).

Feeding behavior

Mice were habituated for one night to the chambers, water bottle, food pellets, and pellet dispensing systems before the first experiments. Prior to the test, mice were fasted (for fast-refeeding tests) overnight (15-20 hours), except Figure 3D in which mice were ad libitum fed (to examine whether activation of EECs can increase food intake). All tests were performed during the light cycle.

To measure food intake during chemogenetic activation of EEC subtypes, triply-transgenic mice (*Marker gene-Cre; Villin-Flp; Rosa*$^{Dual\text{-}hM3D}$ mice or littermate control mice (mice from the same cross that lacked Cre or Flp, and therefore do not express hM3D) were injected intraperitoneally with CNO (1 mg/kg in saline with 1% DMSO) or vehicle (saline with 1% DMSO) and immediately placed into behavior chambers with food pellets and water accessible. After each experiment, pellet consumption was measured by deducting the quantity of pellets left on the ground from the total food count.

For vagotomy experiments, a liquid-diet (0.15 g/ml, Enfamil, ASIN B004L5L5TA) was used instead of food pellets to maintain gastrointestinal flow after vagotomy surgery, and in this case water was not provided.

Conditioned taste aversion (CTA)

All mice were naïve to sucrose or CNO prior to the CTA. Mice were habituated for one night to the chambers and water bottle before the CTA experiment. CTA experiments were performed on 5 consecutive days in Coulbourn behavior chambers during the light cycle.

Prior to each day of CTA, mice were water deprived overnight (15-20 hours). On day 1 and day 3, mice had access to water for 20 min in behavior chamber, followed by an intraperitoneal injection of vehicle. After the injection, mice were placed back to the behavior chambers without water access for another 40 min, and then were returned to their home cage with water/food access for the rest of the day. On day 2, mice were given access to a novel 5%

sucrose solution for 20 min in the same behavior chamber, followed by an injection of antagonist (only for Figure 4C and S4C-S4E) and an injection of CNO or vehicle (for all CTA experiments). After the injection, mice were placed back to the behavior chambers without sucrose access for another 40 min, and then were returned to their home cage with water/food access for the rest of the day. This conditioning was repeated on day 4. On day 5, mice were given access to two bottles (water and 5% sucrose) for 30 min.

To access the conditioned taste aversion, we calculated the choice of sucrose over water during the two-bottle test on day 5, using the sucrose choice index:

$$\text{Choice index (sucrose)} = \text{sucrose licks}/\text{total licks}$$

The sucrose intake ratio was also calculated, comparing sucrose intake after one trial of conditioning (day 4) versus the naïve condition (day 2):

$$\text{Intake ratio (sucrose)} = \text{Sucrose licks}_{Day4}/\text{Sucrose licks}_{Day2}$$

<u>Conditioned flavor preference (CFP)</u>

Prior to the CFP, mice were habituated for one night to the chambers and water bottle. In a separate day, mice were habituated for one night to the flavored solutions in their home cage (with access to regular food and water). All mice were naïve to CNO prior to the experiments. The CFP were performed on 6 consecutive days during the light cycle.

Prior to each day of the CFP experiment, mice were water deprived overnight (15 hours). On day 1, the baseline choice of flavored solution was examined using two-bottle test. Mice were given access to two flavored solution in the Coulbourn behavior chamber for 10 min. These two bottle tests were performed in 4 trials in the same day with about 1 hour between each trial. Positions of the two bottles were swapped in trials 2 & 4 versus trial 1 & 3 to eliminate the effect of bottle's position on animal's preference. The choice of flavor (A or B) was calculated using the total licks across 4 trials:

$$\text{Choice index (flavor B)} = \text{Total licks}_B/(\text{Total licks}_A + \text{Total licks}_B)$$

On day 2 to day 5, training (conditioning) was carried out by coupling one of the flavored solutions with either CNO or vehicle ingestion. Each day, mice were exposed to one of the

610 flavored solutions containing either CNO or vehicle for 2 hours within their home cage (without food and water). After that, mice were kept in home cage without food or water for another 2 hours, before they gained free access to food and water for the rest of the day. On day 2 and day 4, mice were exposed to their preferred flavor (A) containing 0.05% DMSO, while on day 3 and day 5, mice were exposed to their less-preferred flavor (B) containing 0.2 mg/ml CNO and 0.05% DMSO.

On day 6, the choice of flavored solution was examined again using two-bottle test, following the same protocol as day 1. The conditioned flavor preference was accessed by the choice of flavor paired with CNO during conditioned training:

620 $$\text{Choice index (flavor B)} = \text{Total licks}_B / (\text{Total licks}_A + \text{Total licks}_B)$$

The following pairs of flavored solutions were used in CFP (Tan et al., 2020): cherry versus grape flavors, or lemon-lime versus orange flavors. These included: Kool-Aid Lemon-Lime (SKU 00043000955444), 0.5 g/L with 1 mM AceK; Kool-Aid Orange (SKU 00043000955314), 0.5 g/L with 1 mM AceK; Kool-Aid Cherry (SKU 00043000955628), 0.9 g/L with 2 mM AceK; Kool-Aid Grape (SKU 00043000955635), 0.4 g/L with 1 mM AceK.

Pharmacology

To observe the effect of antagonists on feeding response to EEC stimulation, *Marker gene-*
630 *Cre; Villin-Flp; Rosa$^{Dual\text{-}hM3D}$* or littermate control mice were injected intraperitoneally with antagonist/vehicle followed by CNO/vehicle. Immediately after two consecutive injections, mice were placed into behavior chambers with food pellets and water accessible. To observe the effect of antagonists on conditioned taste aversion, antagonist or vehicle was injected intraperitoneally prior to CNO/vehicle injection immediately after 20 min sucrose exposure on day 2 and day 4. For the conditioned flavor preference, antagonist or vehicle was injected intraperitoneally before mice were exposed to the less-preferred flavor with CNO.

Doses were chosen based on previously published reports: devazepide (R&D Systems, 2304) 1 mg/kg in saline with 1% DMSO, 5% Tween 80; ondansetron (Sigma, O3639) 1 mg/kg in
640 saline, JNJ-31020028 (MedChemExpress, HY-14450) 10 mg/kg in saline with 5% DMSO and 5% Tween 80; RP67580 (Tocris, 1635) 1.5 mg/kg in saline with 1% DMSO; Exendin-3 (ApexBio, B6943) 10 ug/mouse in saline.

Behavioral analysis

Behavior data were analyzed with custom Matlab scripts and statistical analyses and bar graphs were generated using Prism. For feeding tests, two trials of the same treatment for each mouse were combined, averaged, and treated as a single replicate. All chemogenetic trials involved age-matched littermates as controls where possible.

650 To calculate pellet food intake, consumption of each pellet was defined as the first pellet removal event after each food pellet delivery. The food dropping ratio ($R_{drop}$) was calculated by the pellets found dropped divided by the total number of pellets removed at the end of each trial:

$$R_{drop} = Pellet_{drop} / Pellet_{removal}$$

At each time point, food intake was estimated by scaling the removed pellet with $R_{drop}$:

$$\text{Food intake} = (1 - R_{drop}) \times \text{Pellet} \times 0.02 \text{ (g/pellet)}$$

EEC quantification

To investigate the identity of EECs labeled by each Cre lines, 30 mm sections of small
660 intestine were prepared and are stained for the reporter and a panel of EEC markers (5-HT, SubP, PYY, CCK, GLP-1, GIP, and SST). The numbers of cell that were labeled by reporter, EEC markers, or both were quantified manually under confocal microscopy (Zeiss, LSM 510), and the overlap between reporter and EEC markers were quantified for villi or crypts separately. The density of cells was reported as number per distance of intestine section (Figure 2-figure supplement 1B, bottom):

$$\text{Density of EEC} = \text{number of EEC} / \text{length of section}$$

Statistical analysis

670 All statistical analyses were performed using GraphPad Prism9. All values are reported as mean ± SEM (error bars or shaded area). Sample size is the number of animal subjects per group and is annotated within Figures or legend. P values for comparisons across multiple groups were performed using analysis of variance (ANOVA) and corrected for multiple comparisons using Sidak multiple comparisons test. In Figures, asterisks denote statistical significance, *$p < 0.05$, **$p < 0.01$, ***$p < 0.001$, ****$p < 0.0001$. # above bars indicate statistical significance comparing with the vehicle control treatment of the same genotype, #$p < 0.05$.

**Acknowledgements**

We thank the UCSF Genomics Core Facility and UCSF Gladstone Transgenic Gene-Targeting Core Laboratory for facility support, and João M. Braz from Allan Basbaum's lab for assistance with the intrathecal injection. We thank Y. Chen, C. Zimmerman, E. Feinberg, J. Garrison, and members of the Knight lab for comments on the manuscript.

Competing interests:

The authors declare that they have no competing interests.

Data and materials availability:

Source data is included in the manuscript. *Villin-Flp* mice will be deposited at Jackson laboratory upon publication.

**Figure 1- Source data 1.** Raw data for Figure 1.

**Figure 2- Source data 1.** Raw data for Figure 2.

**Figure 3- Source data 1.** Raw data for Figure 3C.

**Figure 3- Source data 2.** Raw data for Figure 3F.

**Figure 3- Source data 3.** Raw data for Figure 3G.

**Figure 3- Source data 4.** Raw data for Figure 3I.

**Figure 4- Source data 1.** Raw data for Figure 4B.

**Figure 4- Source data 2.** Raw data for Figure 4C.

**Figure 4- Source data 3.** Raw data for Figure 4D.

**Figure 5- Source data 1.** Raw data for Figure 5B.

**Figure 5- Source data 2.** Raw data for Figure 5C.

**Figure 5- Source data 3.** Raw data for Figure 5D.

**Figure 5- Source data 4.** Raw data for Figure 5E.

**Figure 5- Source data 5.** Raw data for Figure 5F.

**Figure 5- Source data 6.** Raw data for Figure 5G.

**Figure 2- figure supplement 2- Source data 1**. Raw data.

710 **Figure 4- figure supplement 1- Source data 1.** Raw data.

**Figure 5- figure supplement 1- Source data 1.** Raw data.

## References


Adriaenssens, A. E., Reimann, F., & Gribble, F. M. (2018). Distribution and Stimulus Secretion Coupling of Enteroendocrine Cells along the Intestinal Tract. *Compr Physiol, 8*(4), 1603-1638. doi:10.1002/cphy.c170047

Babic, T., & Browning, K. N. (2014). The role of vagal neurocircuits in the regulation of nausea
720 and vomiting. *Eur J Pharmacol, 722*, 38-47. doi:10.1016/j.ejphar.2013.08.047

Bai, L., Mesgarzadeh, S., Ramesh, K. S., Huey, E. L., Liu, Y., Gray, L. A., . . . Knight, Z. A. (2019). Genetic Identification of Vagal Sensory Neurons That Control Feeding. *Cell, 179*(5), 1129-1143 e1123. doi:10.1016/j.cell.2019.10.031

Bellono, N. W., Bayrer, J. R., Leitch, D. B., Castro, J., Zhang, C., O'Donnell, T. A., . . . Julius, D. (2017). Enterochromaffin Cells Are Gut Chemosensors that Couple to Sensory Neural Pathways. *Cell, 170*(1), 185-198 e116. doi:10.1016/j.cell.2017.05.034

Borgmann, D., Ciglieri, E., Biglari, N., Brandt, C., Cremer, A. L., Backes, H., . . . Fenselau, H. (2021). Gut-brain communication by distinct sensory neurons differently controls feeding and glucose metabolism. *Cell Metab, 33*(7), 1466-1482 e1467.
730 doi:10.1016/j.cmet.2021.05.002

Brookes, S. J., Spencer, N. J., Costa, M., & Zagorodnyuk, V. P. (2013). Extrinsic primary afferent signalling in the gut. *Nat Rev Gastroenterol Hepatol, 10*(5), 286-296. doi:10.1038/nrgastro.2013.29

Browne, L. E., Latremoliere, A., Lehnert, B. P., Grantham, A., Ward, C., Alexandre, C., . . . Woolf, C. J. (2017). Time-Resolved Fast Mammalian Behavior Reveals the Complexity of Protective Pain Responses. *Cell Rep, 20*(1), 89-98. doi:10.1016/j.celrep.2017.06.024

Chelikani, P. K., Haver, A. C., & Reidelberger, R. D. (2006). Dose-dependent effects of peptide YY(3-36) on conditioned taste aversion in rats. *Peptides, 27*(12), 3193-3201. doi:10.1016/j.peptides.2006.08.001

740 Clemmensen, C., Muller, T. D., Woods, S. C., Berthoud, H. R., Seeley, R. J., & Tschop, M. H. (2017). Gut-Brain Cross-Talk in Metabolic Control. *Cell, 168*(5), 758-774. doi:10.1016/j.cell.2017.01.025

Deutsch, J. A., & Hardy, W. T. (1977). Cholecystokinin produces bait shyness in rats. *Nature, 266*(5598), 196. doi:10.1038/266196a0

Ervin, G. N., Birkemo, L. S., Johnson, M. F., Conger, L. K., Mosher, J. T., & Menius, J. A., Jr. (1995). The effects of anorectic and aversive agents on deprivation-induced feeding and taste aversion conditioning in rats. *J Pharmacol Exp Ther, 273*(3), 1203-1210. Retrieved from https://www.ncbi.nlm.nih.gov/pubmed/7791092

Ervin, G. N., Carter, R. B., Webster, E. L., Moore, S. I., & Cooper, B. R. (1984). Evidence that
750 taste aversion learning induced by l-5-hydroxytryptophan is mediated peripherally. *Pharmacol Biochem Behav, 20*(5), 799-802. doi:10.1016/0091-3057(84)90202-8

Ervin, G. N., Mosher, J. T., Birkemo, L. S., & Johnson, M. F. (1995). Multiple, small doses of cholecystokinin octapeptide are more efficacious at inducing taste aversion conditioning than single, large doses. *Peptides, 16*(3), 539-545. doi:10.1016/0196-9781(95)00001-z

Ford, A. C., Brandt, L. J., Young, C., Chey, W. D., Foxx-Orenstein, A. E., & Moayyedi, P. (2009). Efficacy of 5-HT3 antagonists and 5-HT4 agonists in irritable bowel syndrome:

systematic review and meta-analysis. *Am J Gastroenterol, 104*(7), 1831-1843; quiz 1844. doi:10.1038/ajg.2009.223

Fothergill, L. J., Callaghan, B., Hunne, B., Bravo, D. M., & Furness, J. B. (2017). Costorage of Enteroendocrine Hormones Evaluated at the Cell and Subcellular Levels in Male Mice. *Endocrinology, 158*(7), 2113-2123. doi:10.1210/en.2017-00243

Fothergill, L. J., & Furness, J. B. (2018). Diversity of enteroendocrine cells investigated at cellular and subcellular levels: the need for a new classification scheme. *Histochem Cell Biol, 150*(6), 693-702. doi:10.1007/s00418-018-1746-x

Gebhart, G. F., & Bielefeldt, K. (2016). Physiology of Visceral Pain. *Compr Physiol, 6*(4), 1609-1633. doi:10.1002/cphy.c150049

Gehart, H., van Es, J. H., Hamer, K., Beumer, J., Kretzschmar, K., Dekkers, J. F., . . . Clevers, H. (2019). Identification of Enteroendocrine Regulators by Real-Time Single-Cell Differentiation Mapping. *Cell, 176*(5), 1158-1173 e1116. doi:10.1016/j.cell.2018.12.029

Gribble, F. M., & Reimann, F. (2016). Enteroendocrine Cells: Chemosensors in the Intestinal Epithelium. *Annual Review of Physiology, Vol 78, 78*, 277-299. doi:10.1146/annurev-physiol-021115-105439

Grun, D., Lyubimova, A., Kester, L., Wiebrands, K., Basak, O., Sasaki, N., . . . van Oudenaarden, A. (2015). Single-cell messenger RNA sequencing reveals rare intestinal cell types. *Nature, 525*(7568), 251-255. doi:10.1038/nature14966

Grunddal, K. V., Ratner, C. F., Svendsen, B., Sommer, F., Engelstoft, M. S., Madsen, A. N., . . . Schwartz, T. W. (2016). Neurotensin Is Coexpressed, Coreleased, and Acts Together With GLP-1 and PYY in Enteroendocrine Control of Metabolism. *Endocrinology, 157*(1), 176-194. doi:10.1210/en.2015-1600

Haber, A. L., Biton, M., Rogel, N., Herbst, R. H., Shekhar, K., Smillie, C., . . . Regev, A. (2017). A single-cell survey of the small intestinal epithelium. *Nature, 551*(7680), 333-339. doi:10.1038/nature24489

Habib, A. M., Richards, P., Cairns, L. S., Rogers, G. J., Bannon, C. A., Parker, H. E., . . . Gribble, F. M. (2012). Overlap of endocrine hormone expression in the mouse intestine revealed by transcriptional profiling and flow cytometry. *Endocrinology, 153*(7), 3054-3065. doi:10.1210/en.2011-2170

Halatchev, I. G., & Cone, R. D. (2005). Peripheral administration of PYY(3-36) produces conditioned taste aversion in mice. *Cell Metab, 1*(3), 159-168. doi:10.1016/j.cmet.2005.02.003

Han, W., Tellez, L. A., Perkins, M. H., Perez, I. O., Qu, T., Ferreira, J., . . . de Araujo, I. E. (2018). A Neural Circuit for Gut-Induced Reward. *Cell, 175*(3), 887-888. doi:10.1016/j.cell.2018.10.018

Hockley, J. R. F., Taylor, T. S., Callejo, G., Wilbrey, A. L., Gutteridge, A., Bach, K., . . . Smith, E. S. J. (2019). Single-cell RNAseq reveals seven classes of colonic sensory neuron. *Gut, 68*(4), 633-644. doi:10.1136/gutjnl-2017-315631

Johnson, S. L., McPhee, L., & Birch, L. L. (1991). Conditioned preferences: young children prefer flavors associated with high dietary fat. *Physiol Behav, 50*(6), 1245-1251. doi:10.1016/0031-9384(91)90590-k

Joyner, K., Smith, G. P., & Gibbs, J. (1993). Abdominal vagotomy decreases the satiating potency of CCK-8 in sham and real feeding. *Am J Physiol, 264*(5 Pt 2), R912-916. doi:10.1152/ajpregu.1993.264.5.R912

Kaelberer, M. M., Buchanan, K. L., Klein, M. E., Barth, B. B., Montoya, M. M., Shen, X., & Bohorquez, D. V. (2018). A gut-brain neural circuit for nutrient sensory transduction. *Science, 361*(6408). doi:10.1126/science.aat5236

Kanoski, S. E., Rupprecht, L. E., Fortin, S. M., De Jonghe, B. C., & Hayes, M. R. (2012). The role of nausea in food intake and body weight suppression by peripheral GLP-1

receptor agonists, exendin-4 and liraglutide. *Neuropharmacology, 62*(5-6), 1916-1927. doi:10.1016/j.neuropharm.2011.12.022

Kern, D. L., McPhee, L., Fisher, J., Johnson, S., & Birch, L. L. (1993). The postingestive consequences of fat condition preferences for flavors associated with high dietary fat. *Physiol Behav, 54*(1), 71-76. doi:10.1016/0031-9384(93)90045-h

Kupari, J., Haring, M., Agirre, E., Castelo-Branco, G., & Ernfors, P. (2019). An Atlas of Vagal Sensory Neurons and Their Molecular Specialization. *Cell Rep, 27*(8), 2508-2523 e2504. doi:10.1016/j.celrep.2019.04.096

Latorre, R., Sternini, C., De Giorgio, R., & Greenwood-Van Meerveld, B. (2016). Enteroendocrine cells: a review of their role in brain-gut communication. *Neurogastroenterol Motil, 28*(5), 620-630. doi:10.1111/nmo.12754

Lewis, J. E., Miedzybrodzka, E. L., Foreman, R. E., Woodward, O. R. M., Kay, R. G., Goldspink, D. A., . . . Reimann, F. (2020). Selective stimulation of colonic L cells improves metabolic outcomes in mice. *Diabetologia, 63*(7), 1396-1407. doi:10.1007/s00125-020-05149-w

Li, C. L., Li, K. C., Wu, D., Chen, Y., Luo, H., Zhao, J. R., . . . Zhang, X. (2016). Somatosensory neuron types identified by high-coverage single-cell RNA-sequencing and functional heterogeneity. *Cell Res, 26*(1), 83-102. doi:10.1038/cr.2015.149

Lin, J. Y., Arthurs, J., & Reilly, S. (2017). Conditioned taste aversions: From poisons to pain to drugs of abuse. *Psychon Bull Rev, 24*(2), 335-351. doi:10.3758/s13423-016-1092-8

Mawe, G. M., & Hoffman, J. M. (2013). Serotonin signalling in the gut--functions, dysfunctions and therapeutic targets. *Nat Rev Gastroenterol Hepatol, 10*(8), 473-486. doi:10.1038/nrgastro.2013.105

McFarlane, M. R., Brown, M. S., Goldstein, J. L., & Zhao, T. J. (2014). Induced ablation of ghrelin cells in adult mice does not decrease food intake, body weight, or response to high-fat diet. *Cell Metab, 20*(1), 54-60. doi:10.1016/j.cmet.2014.04.007

Mishra, S. K., & Hoon, M. A. (2010). Ablation of TrpV1 neurons reveals their selective role in thermal pain sensation. *Mol Cell Neurosci, 43*(1), 157-163. doi:10.1016/j.mcn.2009.10.006

Morarach, K., Mikhailova, A., Knoflach, V., Memic, F., Kumar, R., Li, W., . . . Marklund, U. (2021). Diversification of molecularly defined myenteric neuron classes revealed by single-cell RNA sequencing. *Nat Neurosci, 24*(1), 34-46. doi:10.1038/s41593-020-00736-x

Myers, K. P., & Sclafani, A. (2006). Development of learned flavor preferences. *Dev Psychobiol, 48*(5), 380-388. doi:10.1002/dev.20147

Najjar, S. A., Davis, B. M., & Albers, K. M. (2020). Epithelial-Neuronal Communication in the Colon: Implications for Visceral Pain. *Trends Neurosci, 43*(3), 170-181. doi:10.1016/j.tins.2019.12.007

Park, S. I., Brenner, D. S., Shin, G., Morgan, C. D., Copits, B. A., Chung, H. U., . . . Rogers, J. A. (2015). Soft, stretchable, fully implantable miniaturized optoelectronic systems for wireless optogenetics. *Nat Biotechnol, 33*(12), 1280-1286. doi:10.1038/nbt.3415

Perez, C., & Sclafani, A. (1991). Cholecystokinin conditions flavor preferences in rats. *Am J Physiol, 260*(1 Pt 2), R179-185. doi:10.1152/ajpregu.1991.260.1.R179

Polyak, S., Mah, C., Porvasnik, S., Herlihy, J. D., Campbell-Thompson, M., Byrne, B. J., & Valentine, J. F. (2008). Gene delivery to intestinal epithelial cells in vitro and in vivo with recombinant adeno-associated virus types 1, 2 and 5. *Dig Dis Sci, 53*(5), 1261-1270. doi:10.1007/s10620-007-9991-1

Raybould, H. E. (2007). Mechanisms of CCK signaling from gut to brain. *Curr Opin Pharmacol, 7*(6), 570-574. doi:10.1016/j.coph.2007.09.006

Reynaud, Y., Fakhry, J., Fothergill, L., Callaghan, B., Ringuet, M., Hunne, B., . . . Furness, J. B. (2016). The chemical coding of 5-hydroxytryptamine containing enteroendocrine

cells in the mouse gastrointestinal tract. *Cell Tissue Res, 364*(3), 489-497. doi:10.1007/s00441-015-2349-7

Savastano, D. M., & Covasa, M. (2007). Intestinal nutrients elicit satiation through concomitant activation of CCK(1) and 5-HT(3) receptors. *Physiol Behav, 92*(3), 434-442. doi:10.1016/j.physbeh.2007.04.017

Sclafani, A., & Ackroff, K. (2012). Role of gut nutrient sensing in stimulating appetite and conditioning food preferences. *Am J Physiol Regul Integr Comp Physiol, 302*(10), R1119-1133. doi:10.1152/ajpregu.00038.2012

Sharma, N., Flaherty, K., Lezgiyeva, K., Wagner, D. E., Klein, A. M., & Ginty, D. D. (2020). The emergence of transcriptional identity in somatosensory neurons. *Nature, 577*(7790), 392-398. doi:10.1038/s41586-019-1900-1

Slotnick, B. (2009). A simple 2-transistor touch or lick detector circuit. *J Exp Anal Behav, 91*(2), 253-255. doi:10.1901/jeab.2009.91-253

Smith, G. P., Jerome, C., Cushin, B. J., Eterno, R., & Simansky, K. J. (1981). Abdominal vagotomy blocks the satiety effect of cholecystokinin in the rat. *Science, 213*(4511), 1036-1037. doi:10.1126/science.7268408

Spohn, S. N., & Mawe, G. M. (2017). Non-conventional features of peripheral serotonin signalling - the gut and beyond. *Nat Rev Gastroenterol Hepatol, 14*(7), 412-420. doi:10.1038/nrgastro.2017.51

Sykaras, A. G., Demenis, C., Cheng, L., Pisitkun, T., McLaughlin, J. T., Fenton, R. A., & Smith, C. P. (2014). Duodenal CCK cells from male mice express multiple hormones including ghrelin. *Endocrinology, 155*(9), 3339-3351. doi:10.1210/en.2013-2165

Tan, H. E., Sisti, A. C., Jin, H., Vignovich, M., Villavicencio, M., Tsang, K. S., . . . Zuker, C. S. (2020). The gut-brain axis mediates sugar preference. *Nature, 580*(7804), 511-516. doi:10.1038/s41586-020-2199-7

Williams, E. K., Chang, R. B., Strochlic, D. E., Umans, B. D., Lowell, B. B., & Liberles, S. D. (2016). Sensory Neurons that Detect Stretch and Nutrients in the Digestive System. *Cell, 166*(1), 209-221. doi:10.1016/j.cell.2016.05.011

Yamamoto, T., & Ueji, K. (2011). Brain mechanisms of flavor learning. *Front Syst Neurosci, 5*, 76. doi:10.3389/fnsys.2011.00076

Ye, L., Bae, M., Cassilly, C. D., Jabba, S. V., Thorpe, D. W., Martin, A. M., . . . Rawls, J. F. (2021). Enteroendocrine cells sense bacterial tryptophan catabolites to activate enteric and vagal neuronal pathways. *Cell Host Microbe, 29*(2), 179-196 e179. doi:10.1016/j.chom.2020.11.011

# Figure 1

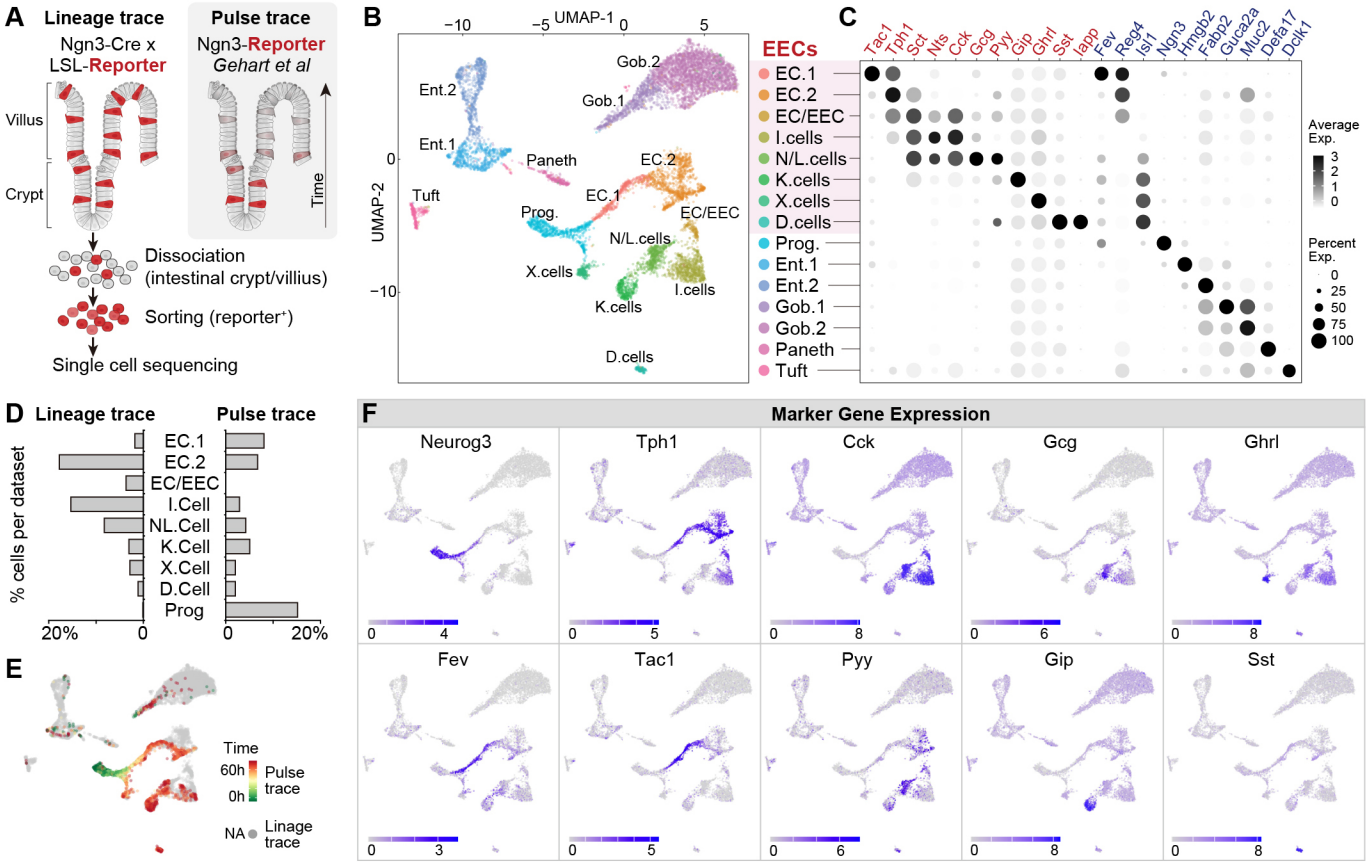


**Figure 1. Molecular diversity of intestinal EECs**

(A) Overview of strategies to enrich EECs for the scRNA-Seq. Lineage-trace or pulse-trace strategies permanently or transiently label EECs that are derived from *Neurog3*⁺ progenitors.
(B) Uniform manifold approximation and projection (UMAP) plots indicating cell subtype diversity across 9338 intestinal epithelium cells. This includes 8 clusters of EEC subtypes (3412 cells, with 2168 lineage-traced cells and 1244 pulse-traced cells), progenitors, enterocytes, goblet cells, tuft cells, and Paneth cells.
(C) Dot plot of expression of gut hormones (red) and cell type marker genes (blue).
(D) Distribution of lineage-trace and pulse-trace cells across EEC subtypes. Lineage-trace strategy avoided early stage cells (progenitors), while pulse-trace did not label the EC-EEC cluster.
(E) Differentiation time (pulse-trace dataset) color-coded on UMAP map.
(F) Expression of EEC cluster marker genes. UMAP plots show cells colored by gene expression using ln(TPM+1), TPM: transcripts per million.

See also Figure 1-figure supplement 1 and Figure 1-source data 1.

# Figure 2

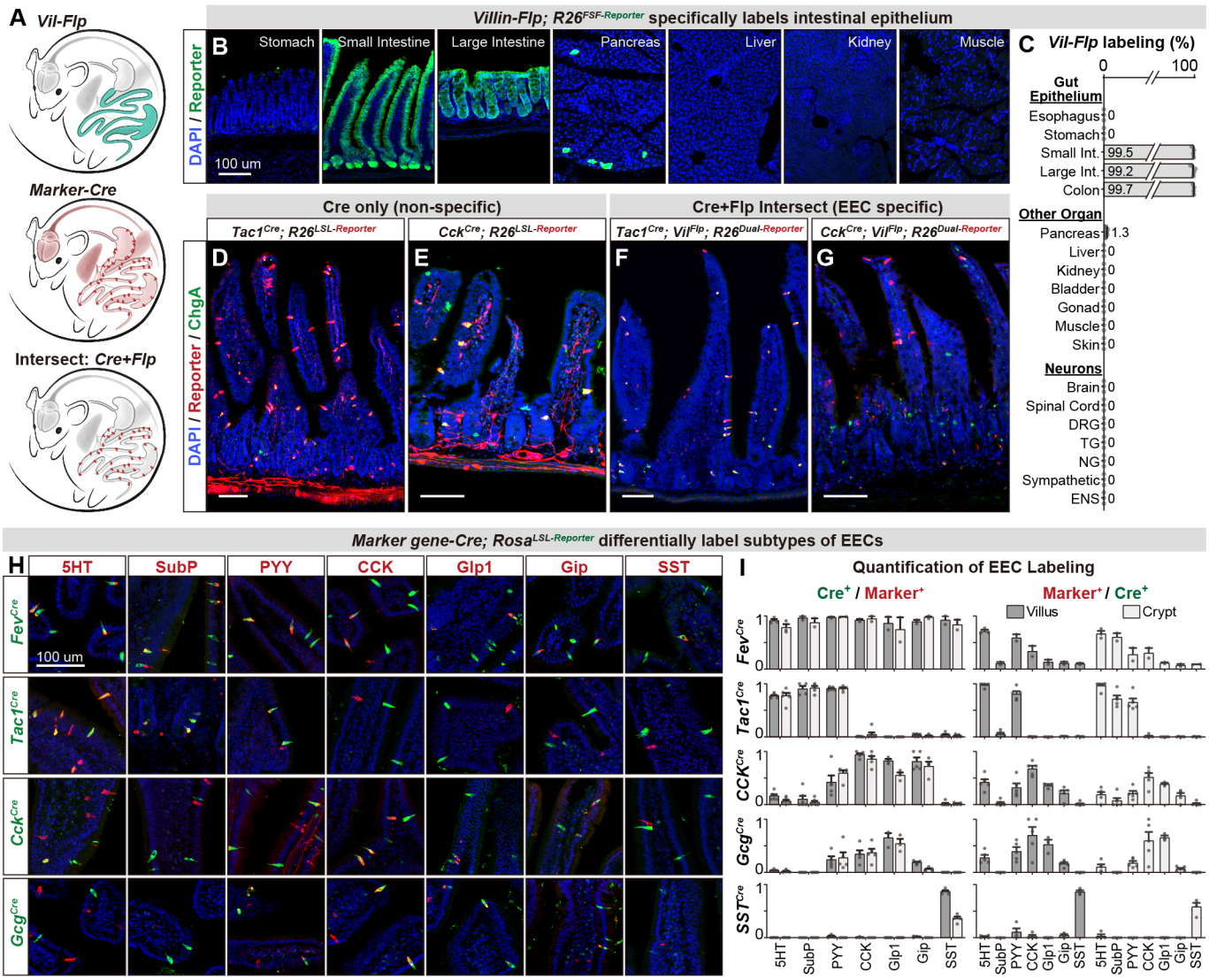


**Figure 2. An intersectional genetic approach to selectively target EEC subtypes**

(A) Schematic comparing the labeling patterns of *Vil-Flp*, *Marker gene-Cre*, and their intersection.
(B) Cross section of organs shows that *Vil-Flp* promotes recombination and reporter expression in the intestinal epithelium, as well as very small subsets of pancreatic cells.
(C) Quantification of the *Vil-Flp* labeling across the GI tract, other visceral organs, and neuronal tissues.
(D-G) Cross sections of the small intestines reveal the expression pattern of reporter using either single *Marker gene-Cre* lines (D-E) or the *Marker gene-Cre*; *Vil-Flp* intersectional strategy (F-G). *Tac1*$^{Cre}$ (D) and *Cck*$^{Cre}$ (E) label not only EECs but also other cell types, including neuronal terminals and cell bodies in the intestine. In contrast, the labeling of the intersectional strategy is restricted to EECs (F-G). ChgA staining (green) marks the majority of enterochromaffin cells and subsets of EECs.
(H) Double immunostaining of hormonal marker genes (red) and Cre-induced reporter (green) on small intestine villus sections of various *Marker gene-Cre; R26*$^{LSL\text{-}Reporter}$ mice.
(I) Quantification of EEC labeling across villi and crypts using various *Marker gene-Cre*; *RosaLSL-Reporter* mice (for 2H and S2A). Left shows the ratio of EEC subtypes (Marker$^{+}$) that are labeled by each *Cre* line. Right indicates the composition of cells in villi versus crypts that are labeled by each *Marker gene-Cre* line.

Values are reported as mean ± SEM. Scale bar: 100 µm. See also Figure 2-figure supplement 1 and 2, and Figure 2- source data 1.

# Figure 3

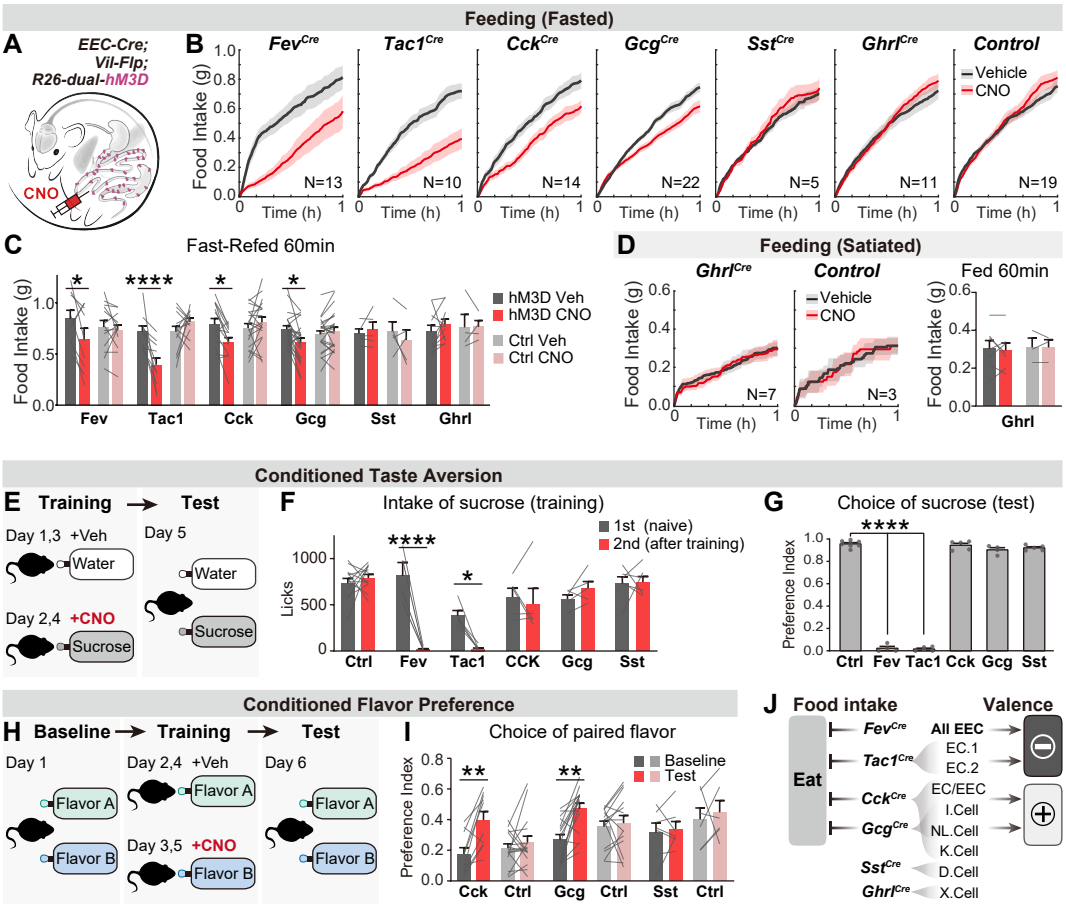


**Figure 3. Distinct EEC subtypes signal reward and aversion**

(A) Overview of the chemogenetic approach to stimulate EEC subtypes. Littermates that were Cre or Flp negative (and therefore did not express hM3D) were used as genetic controls.
(B) Cumulative food intake of overnight food-deprived mice, comparing trials with CNO or saline treatment.
(C) Quantification of total food intake at 1 hour from (B).
(D) Cumulative food intake of satiated mice, and quantification of total food intake at 1 hour.
(E) CTA paradigm. In the training trials, CNO or vehicle is delivered intraperitoneally after 20 min of sucrose or water ingestion.
(F) Total sucrose intake during training trials of CTA, comparing 1st trial (day 1, naïve mice) versus 2nd trial (day 3, after pairing with CNO for one trial).
(G) Choice of sucrose during the test trial of CTA (day 5).
(H) CFP paradigm. In the training trials, CNO or vehicle is delivered in drinking solution with flavor A or flavor B.
(I) Choice of the CNO paired flavor before versus after CFP training.
(J) Summary of EEC subtypes labeled by each Cre line, and their regulation of food intake and food learning.

Values are reported as mean ± SEM. N mice is annotated within figures. *P < 0.05, **P < 0.01, ***P < 0.001, ****P < 0.0001, two-way ANOVA (C, D, G, and I) or Ordinary one-way ANOVA (F).

See also Figure 3-source data 1-4.

# Figure 4

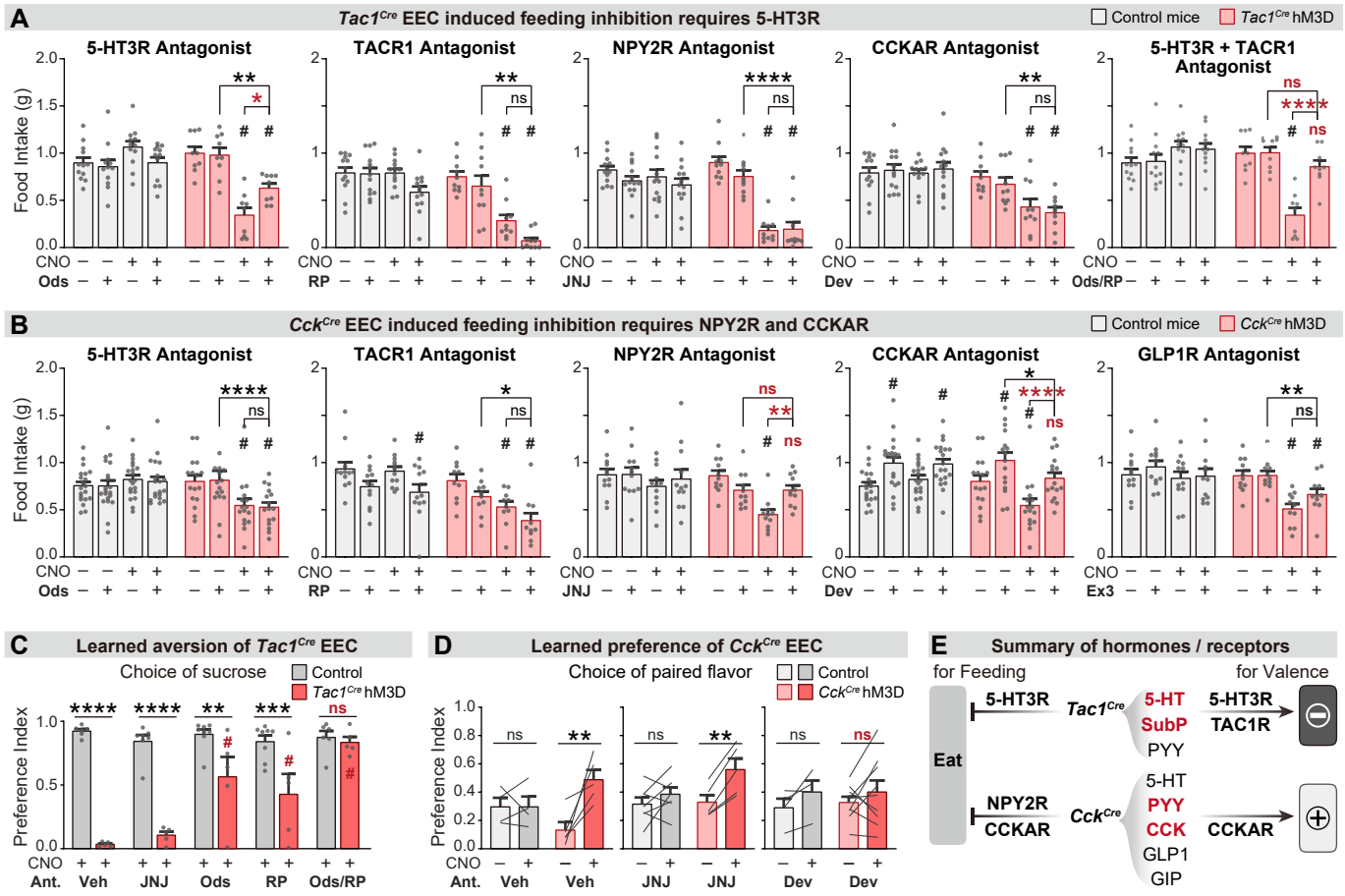


**Figure 4. Different neurotransmitters regulate food consumption and learning**

(A-B) One-hour food intake of overnight food-deprived mice. Quantification compares trials treated with CNO, antagonist, or vehicle before the start of feeding, using *Tac1*$^{Cre}$*; Vil-Flp; R26*$^{Dual\text{-}hM3D}$ mice (B), *Cck*$^{Cre}$*; Vil-Flp; R26*$^{Dual\text{-}hM3D}$ mice (C), or control mice (B-C).
(C) Choice of sucrose during the test trial of CTA. Quantification compares *Tac1*$^{Cre}$*; Vil-Flp; R26*$^{Dual\text{-}hM3D}$ mice and control mice that are treated with antagonist or vehicle before CTA training. All mice received CNO during CTA training.
(D) Choice of the CNO-paired flavor before versus after CTP training, using *Cck*$^{Cre}$*; Vil-Flp; R26*$^{Dual\text{-}hM3D}$ mice. Antagonist or vehicle was delivered before each CFP training trial.
(E) Summary of gut hormones expressed in the *Tac1*$^{Cre}$ EECs or *Cck*$^{Cre}$ EECs, and the corresponding receptors that mediate the regulation of feeding behavior.

Values are reported as mean ± SEM. *P < 0.05, **P < 0.01, ***P < 0.001, ****P < 0.0001; # or ns above bars indicate p-value comparing with the vehicle control treatment of the same genotype (#p < 0.05); two-way ANOVA. See also Figure 4-figure supplement 1 and 2, and Figure 4-source data 1-3.

# Figure 5

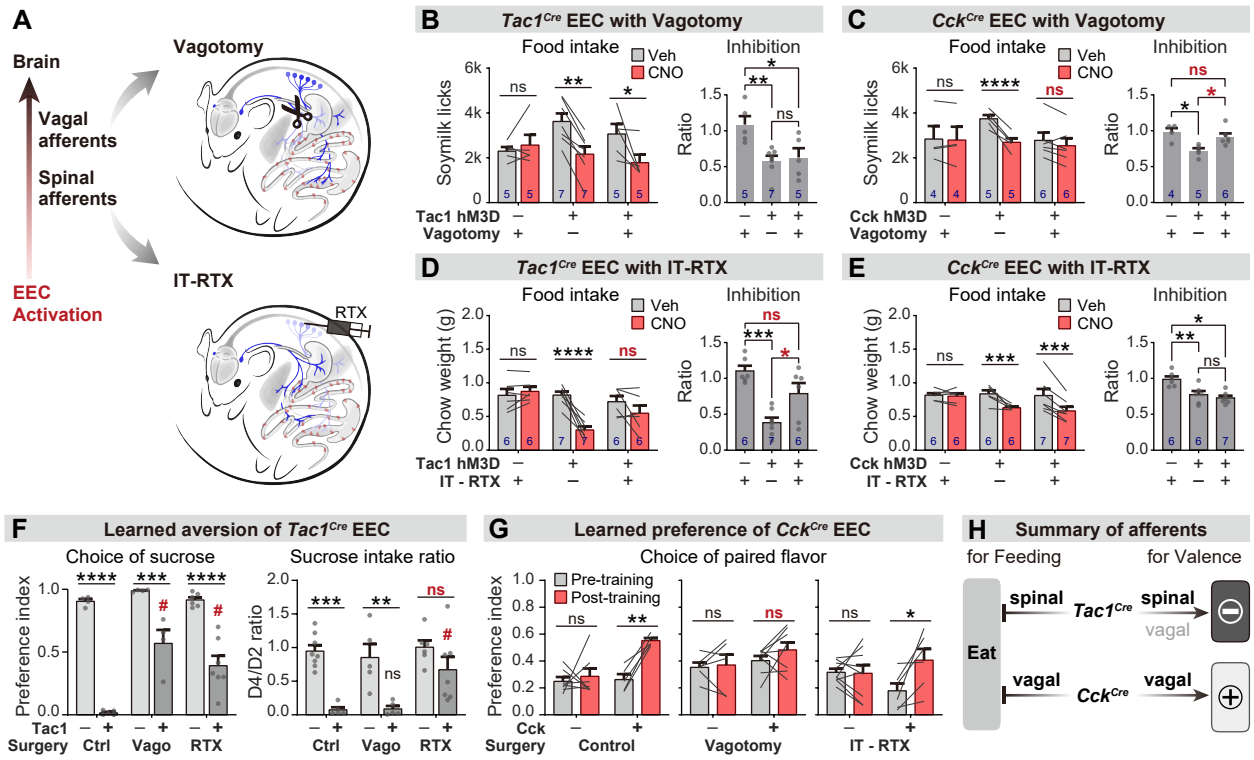


**Figure 5. Parallel neuronal pathways convey EEC signals to the brain**

(A) Overview of surgical and chemical approaches to disrupt neuronal pathways connecting EECs to the brain.
(B-D) One-hour food intake after overnight food deprivation, testing *Tac1*$^{Cre}$*; Vil-Flp; R26*$^{Dual\text{-}hM3D}$ mice (B or D) or *Cck*$^{Cre}$*; Vil-Flp; R26*$^{Dual\text{-}hM3D}$ mice (C or E), with subdiaphragmatic vagotomy (B-C) or IT-RTX treatment (C-E). Left: comparison of food intake after treatment with CNO or vehicle. Right: ratio of feeding inhibition after treatment with CNO versus vehicle.
(F) Quantification of CTA comparing *Tac1*$^{Cre}$*; Vil-Flp; R26*$^{Dual\text{-}hM3D}$ mice and control mice that received sham treatment, vagotomy, or IT-RTX before CTA training. All mice received CNO during CTA training. Left: Choice of sucrose in the test trial. (D) Ratio of total sucrose intake in the 2nd sucrose trial (day 3, after pairing with CNO for one trial) versus 1st sucrose trial (day 1, naïve mice). Of note, the apparent increased choice of sucrose after vagotomy is largely due to the low ingestion of water; see also Figure S4I.
(G) Choice of CNO paired flavor before versus after CFP training, using *Cck*$^{Cre}$*; Vil-Flp; R26*$^{Dual\text{-}hM3D}$ mice. Sham treatment, vagotomy, or IT-RTX was performed before the CFP.
(H) Summary of neuronal pathways required for *Tac1*$^{Cre}$ EECs or *Cck*$^{Cre}$ EECs to regulate food intake or food learning.

Values are reported as mean ± SEM. *P < 0.05, **P < 0.01, ***P < 0.001, ****P < 0.0001; # or ns above bars indicate p-value comparing with the vehicle control treatment of the same genotype (#p < 0.05); two-way ANOVA (left of B-E; F, G), or ordinary one-way ANOVA (right of B-E). See also Figure 5-figure supplement 1 and Figure 5-source data 1-6.

# Figure 1- Figure supplement 1

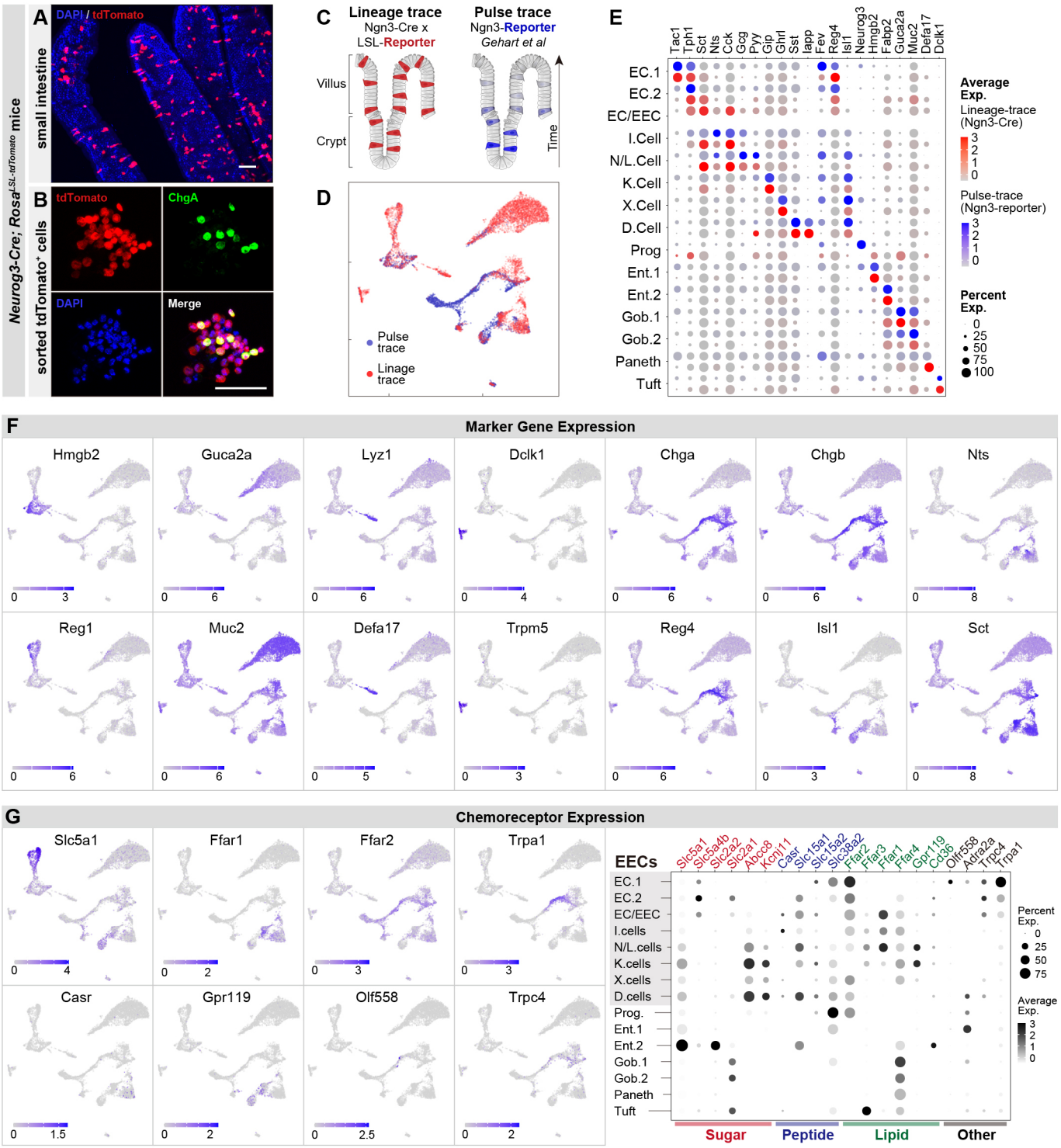


**Figure 1- FIgure Supplement 1. Molecular diversity of intestinal EECs.**

(A-B) Using *Neurog3-Cre; Rosa*$^{LSL\text{-}tdTomato}$ mice, the expression of tdTomato permanently labels EECs across villi of small intestine (A) and after fluorescence-activated cell sorting (B).
(C-D) Comparison of EECs enriched with the strategy of lineage-trace versus pulse-trace. UMAP plots shows cells colored by the origin of datasets (D).
(E) Dot plot demonstrating that the expression of gut hormones and cell type marker genes are conserved across lineage-trace dataset (red) versus pulse-trace dataset (blue).
(F) Expression of marker genes of enterocytes, goblet cells, Paneth cells, tuft cells, and EECs. UMAP plots show cells colored by gene expression using ln(TPM+1).
(G) Expression of genes for the detection or absorption of nutrients and other chemical signals. Left: UMAP plots show cells colored by gene expression using ln(TPM+1). Right: dot plot shows gene expression across clusters.

Scale bar: 50 μm.

# Figure 2- Figure Supplement 2

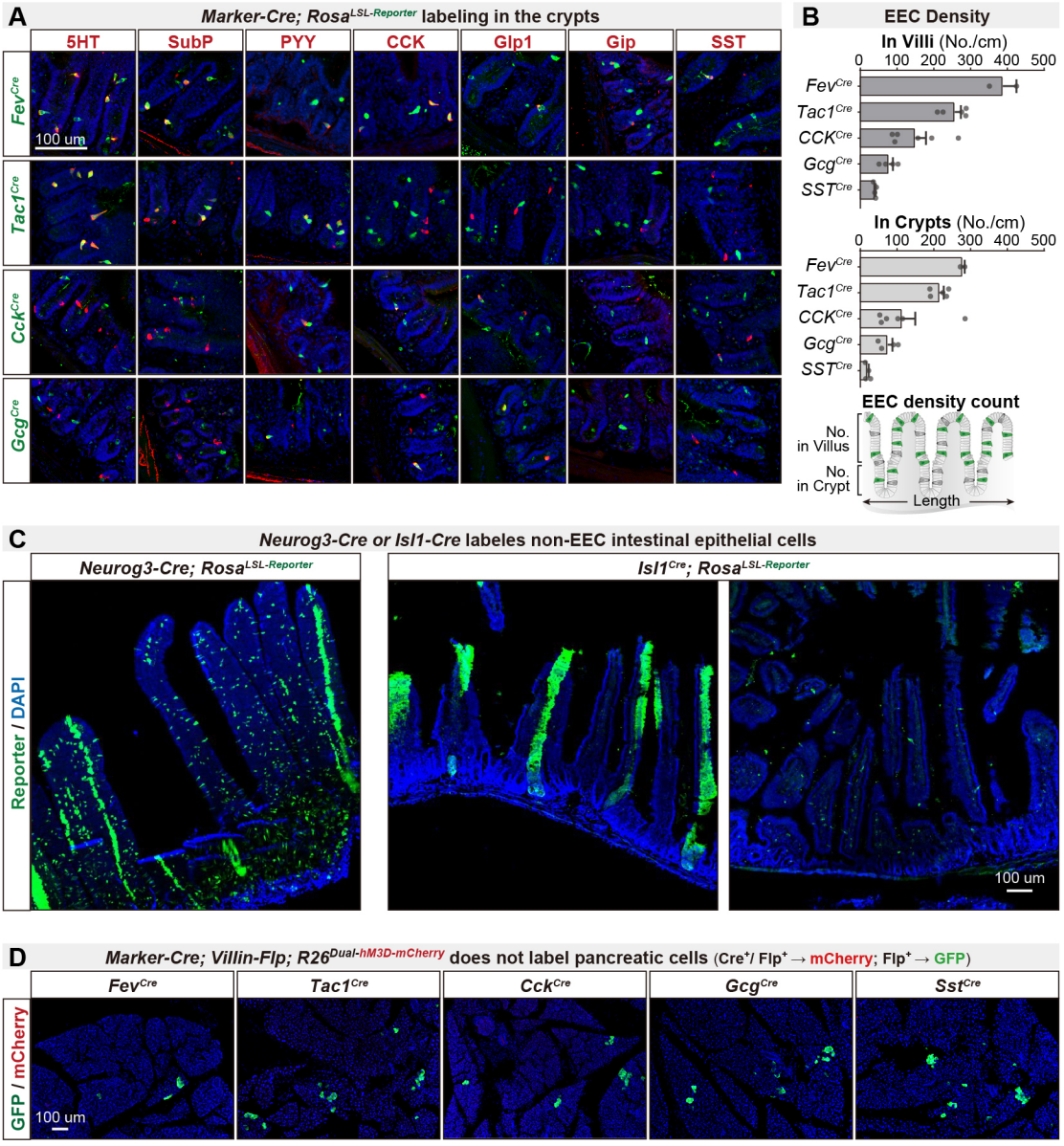


**Figure 2- Figure Supplement 2. An intersectional genetic approach to selectively target EEC subtypes.**

(A) Double immunostaining of hormonal marker genes (red) and Cre-induced reporter (green) on small intestine crypt sections of various *Marker-Cre; Rosa*$^{LSL\text{-}Reporter}$ mice.
(B) Quantification of EEC labeling across villi and crypts using various *Marker-Cre; Rosa*$^{LSL\text{-}Reporter}$ mice. Bottom: schematic of quantification strategy, using 30um-thick sections of small intestine.
(C) Cross sections of the small intestine reveal the expression pattern of reporter using *Neurog3-Cre; Rosa*$^{LSL\text{-}Reporter}$ (left) or *Isl1Cre; Rosa*$^{LSL\text{-}Reporter}$ (right).
(D) Cross sections of the pancreas reveal the expression pattern of GFP and mCherry using various *Marker-Cre; Vil-Flp; R26*$^{Dual\text{-}hM3D\text{-}mCherry}$ mice. Of note, GFP expression is induced by Flp recombination and was observed in a small subset of pancreatic cells. mCherry expression is induced by the combination of Flp and Cre and was not observed in any pancreatic cells.

Values are reported as mean ± SEM. Scale bar: 100 µm. See also Figure 2-Figure Supplement 2-source data 1

# Figure 4- Figure Supplement 1

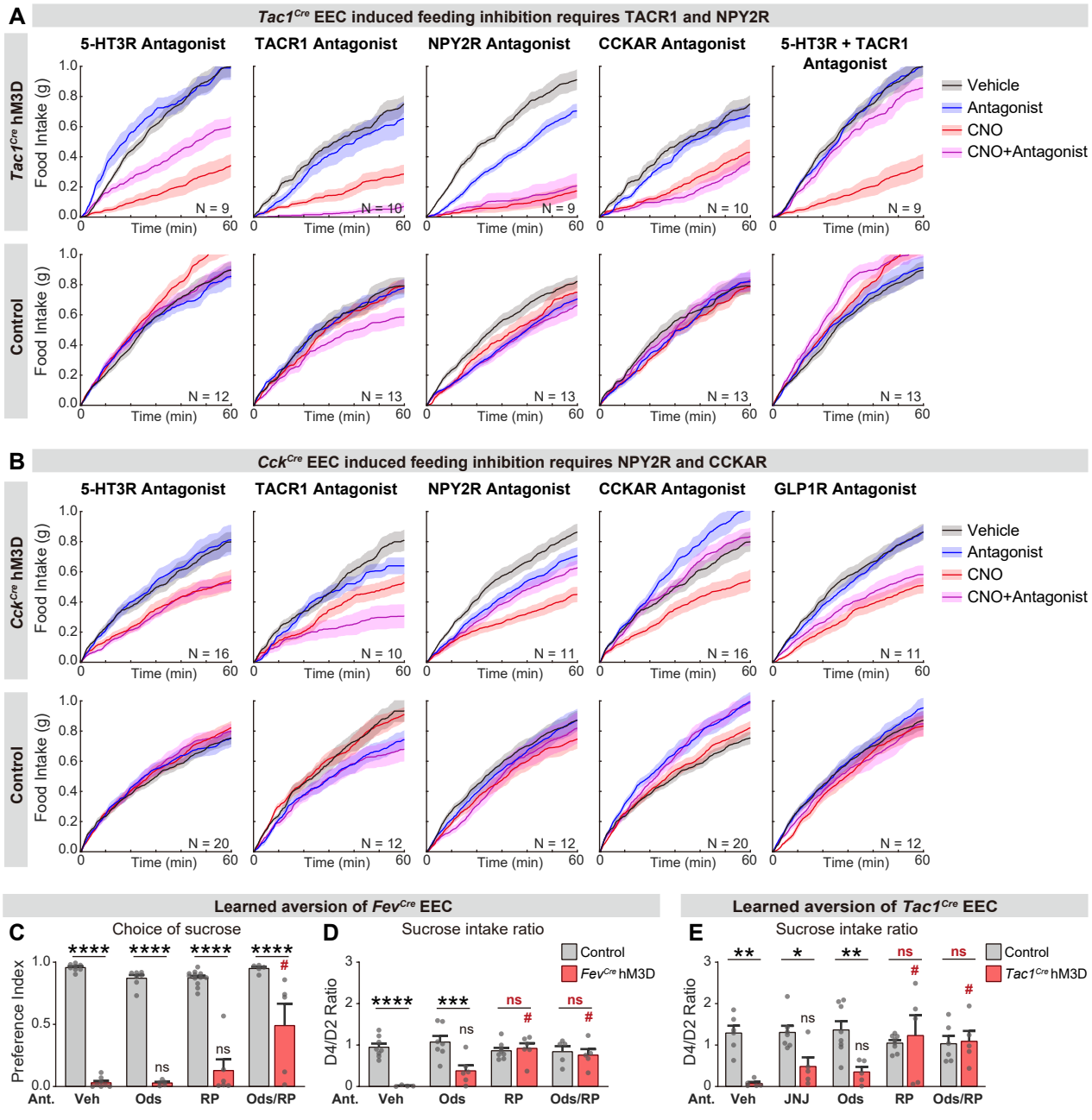


**Figure 4- FIgure Supplement 1. Different neurotransmitters regulate food consumption and learning.**

(A-B) Cumulative food intake of overnight food-deprived mice. Each plot compares trials with CNO, antagonist, or vehicle treatment, using either *Tac1*$^{Cre}$*; Vil-Flp; R26*$^{Dual\text{-}hM3D}$ mice (A), *Cck*$^{Cre}$*; Vil-Flp; R26*$^{Dual\text{-}hM3D}$ mice (B), or control mice (A-B).
(C-D) Quantification of CTA comparing *Fev-Cre; Vil-Flp; R26*$^{Dual\text{-}hM3D}$ mice and control mice that are treated with antagonist or vehicle before CTA training. All mice received CNO during CTA training. (C) Choice of sucrose during the test trial of CTA. (D) Ratio of total sucrose intake in the 2nd sucrose trial (day 3, after pairing with CNO for one trial) versus 1st sucrose trial (day 1, naïve mice)
(E) Quantification of CTA comparing *Tac1*$^{Cre}$*; Vil-Flp; R26*$^{Dual\text{-}hM3D}$ mice and control mice that are treated with antagonist or vehicle before CTA training. All mice received CNO during CTA training. Plot shows the ratio of total sucrose intake in the 2nd sucrose trial (day 3, after pairing with CNO for one trial) versus 1st sucrose trial (day 1, naïve mice)

Values are reported as mean ± SEM. *P < 0.05, **P < 0.01, ***P < 0.001, ****P < 0.0001; # or ns above the bar indicate p-value comparing with the vehicle control treatment of the same genotype (#p < 0.05); two-way ANOVA. See also Figure 4-figure supplement 1-source data 1.

# Figure 5- Figure Supplement 1

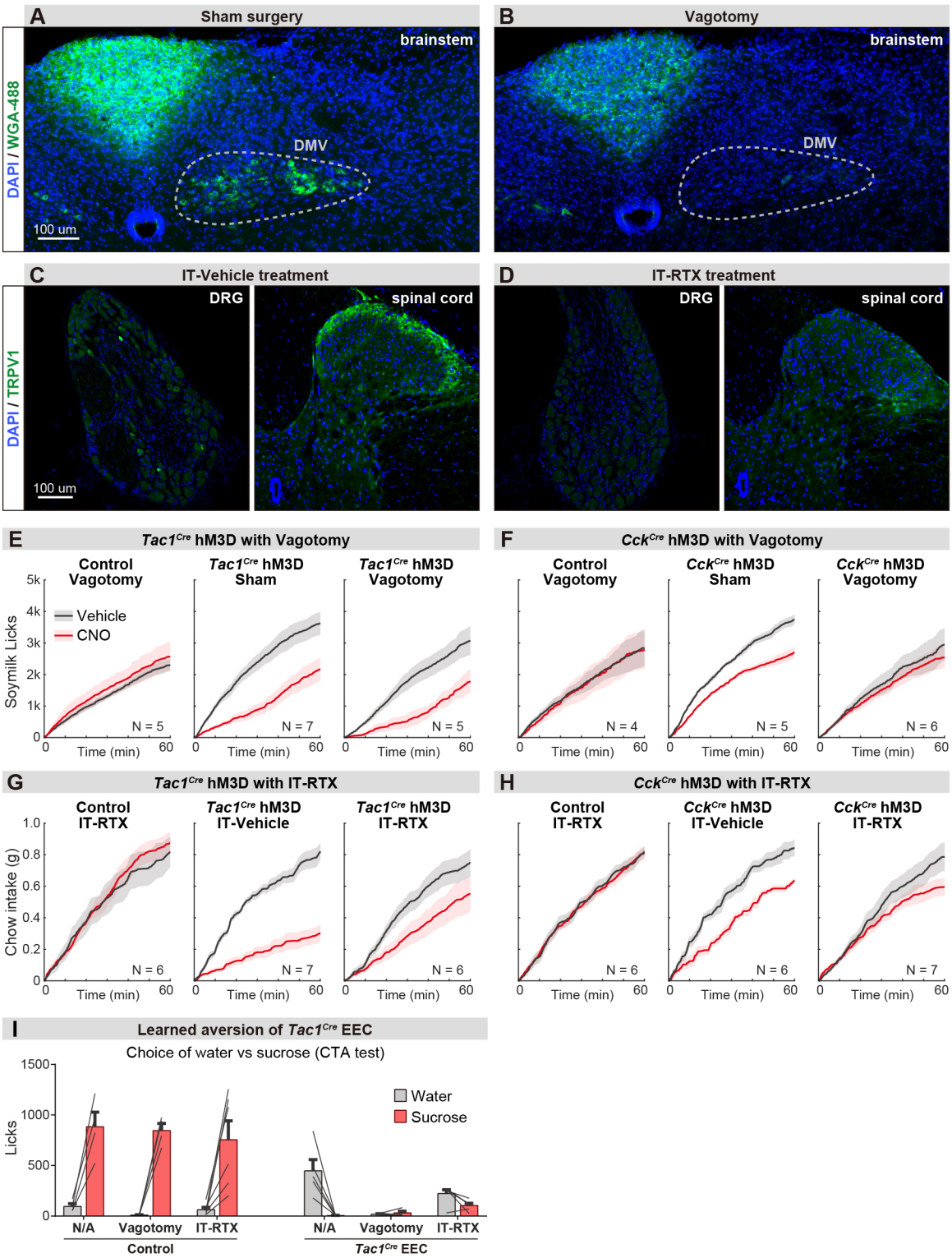


**Figure 5, Figure Supplement 1. Parallel neuronal pathways convey EEC signals to the brain.**

(A-B) Brainstem sections showing the vagal motor neurons that are labeled by intraperitoneal injection of wheat germ agglutinin (WGA-488). Labeling was largely absent following subdiaphragmatic vagotomy (B) compared with sham control (A).
(C-D) Immunostaining of TRPV1 on DRG and spinal cord sections. The TRPV1$^{+}$ DRG neurons (left) and axonal terminals in spinal cord (right) are greatly diminished following the intrathecal injection of RTX (D) compared with vehicle injection (C).
(E-H) Cumulative food intake over time after overnight food deprivation. Each plot compares trials with CNO or vehicle treatment, using either *Tac1$^{Cre}$; Vil-Flp; R26$^{Dual\text{-}hM3D}$* mice (E, G), *Cck$^{Cre}$; Vil-Flp; R26$^{Dual\text{-}hM3D}$* mice (F, H), or control mice (E-H), with vagotomy versus sham treatment (E-F), or IT-RTX versus IT-vehicle treatment (G-H).
(I) Licks of sucrose versus water during CTA choice test, using *Tac1$^{Cre}$; Vil-Flp; R26$^{Dual\text{-}hM3D}$* mice or control mice with sham treatment, vagotomy, or IT-RTX. Of note, stimulation of *Tac1$^{Cre}$* EEC in the vagotomy mice reduced the intake of both sucrose and water, suggesting vagotomy is not sufficient to block the aversion induced by *Tac1$^{Cre}$* EECs.

Values are reported as mean ± SEM. Scale bar: 100 μm. See also Figure 5-figure supplement 1-source data 1.